UNCLASSIFIED

AD NUMBER

AD809702

LIMITATION CHANGES

TO:

Approved for public release; distribution is unlimited.

FROM:

**Distribution authorized to U.S. Gov't. agencies and their contractors;
Administrative/Operational Use; 31 JAN 1967.
Other requests shall be referred to Air Force Technical Applications Center, Washington, DC 20333.**

AUTHORITY

AFTAC ltr 25 Jan 1972

THIS PAGE IS UNCLASSIFIED

809702

THIS DOCUMENT IS SUBJECT TO SPECIAL EXPORT CONTROLS AND EACH TRANSMITTAL TO FOREIGN GOVERNMENTS OR FOREIGN NATIONAL MAY BE MADE ONLY WITH PRIOR APPROVAL OF CHIEF, AFTAC.

SCIENCE SERVICES DIVISION

TEXAS INSTRUMENTS
INCORPORATED

AFTAC Project VT/4053

ARRAY RESEARCH
ARRAY PROCESSING AT UBO
Special Report No. 22

by

George C. Burrell, Program Manager
Paul R. Lintz

TEXAS INSTRUMENTS INCORPORATED
Science Services Division
P. O. Box 5621
Dallas, Texas 75222

Contract No. AF 33(657)-12747
Date of Contract: 13 November 1963
Contract Expiration Date: 20 January 1967

Prepared for

AIR FORCE TECHNICAL APPLICATIONS CENTER
VELA SEISMOLOGICAL CENTER
Washington, D.C. 20333

ARPA Order No. 104-60
Project Code No. 8100

31 January 1967

TABLE OF CONTENTS

Section	Title	Page
I	INTRODUCTION	1
II	UBO NOISE PREDICTION STUDY	2
	A. SUMMARY	2
	B. PRESENTATION OF RESULTS	3
III	ANALOG PROCESSORS AT UBO	25
	A. MULTICHANNEL PROCESSORS AT UBO	25
	B. FILTER DESIGN AND DESIGNATION	26
IV	ROAD NOISE FILTER DESIGN AND IMPLEMENTATION PROBLEMS	29
	A. UBO ROAD NOISE	29
	B. SYNTHESIS OF ROAD NOISE FILTERS	31
V	THEORETICAL FILTER EVALUATION	36
	A. HIGH-NOISE FILTER	36
	B. ENSEMBLE FILTER	42
	C. EVALUATION SUMMARY	42
VI	EVALUATION OF THE ON-LINE PROCESSORS	48
	A. EVALUATION OF IP-1, IP-2, MCF-9, AND DG 1-4	48
	B. EVALUATION OF THE ROAD NOISE FILTER	48

LIST OF TABLES

Table	Title	Page
1	Filter Design Parameters	5
2	10-Channel MAP Filters (Surface Array)	27
3	19-Channel MAP Filters (Subsurface Array)	28

LIST OF ILLUSTRATIONS

Figure	Description	Page
1	Artist's Concept of UBO Array Complex	6
2	Power Density Spectra of the Center Seismometer for the Surface Array (Z 10) and for the Subsurface Array (SZ 10) for Noise Sample A (NSA), Noise Sample B (NSB) and Noise Sample C (NSC)	7
3a	A Short Portion of NSA Complete With the Output of the MCF's SP1, SP2, SP3, and SP4, and Their Error Traces	8
3b	Enlargement of Traces 10 through 21 in Figure 3a	8
4	Power Spectra Plots of $\frac{N_i - N_p}{N_i}$ for MCF's SP1 SP2, SP3 and SP4, Noise Sample A	9
5a	A Short Portion of NSA Traces 10 through 21 are the Reference Trace Z 10, the Predicted Traces and the Error Traces for MCF's P1, P2, P3 and P4	10
5b	Enlargement of Traces 10 Through 21 in Figure 5a	10
6	Power Spectra Plots of $\frac{N_i - N_p}{N_i}$ for MCF's P1, P2, P3 and P4, Noise Sample A	11
7a	A Short Portion of NSA, With the Output of the MCF's SSP1 through SSP4, and Error and Reference Traces	12
7b	Enlargement of Traces 10 through 21 in Figure 7a	12
8	Power Spectra Plots of $\frac{N_i - N_p}{N_i}$ for MCF's SSP1, SSP2, SSP3, and SSP4, Noise Sample A	13
9	Power Spectra Plots of $\frac{N_i - N_p}{N_i}$ for MCF's P1, P2, P3, P4, SSP1, SSP2, SSP3, and SSP4, Noise Sample A	14
10	A Short Portion of Subsurface NSB, With the Outputs of MCF's SP5 and SP6, Reference Traces (SZ 10), and Error Traces	15
11	Power Spectra Plots of $\frac{N_i - N_p}{N_i}$ for MCF's SP5 and SP6, Noise Sample B	16

LIST OF ILLUSTRATIONS

Figure	Description	Page
12a	A Short Portion of NSB (Surface), With the Output of MCF's P5, P6, SSP5, and SSP6, Reference Traces and Error Traces	17
12b	Enlargement of Traces 10 Through 21 in Figure 12a	17
13	Power Spectra Plots of $\frac{N_i - N_p}{N_i}$ for MCF's P5, P6, SSP5, and SSP6, Noise Sample B	18
14	A Short Portion of NSC (Subsurface) With the Output of MCF's SP7 and SP8, Reference Traces, and Error Traces	19
15	Power Spectra Plots of $\frac{N_i - N_p}{N_i}$ for MCF's SP7 and SP8, Noise Sample C	20
16a	A Short Portion of NSC (Surface) with the Outputs of MCF's P7, P8, SSP7, SSP8, Reference Traces, and Error Traces	21
16b	Enlargement of Traces 10 Through 21 in Figure 12a	21
17	Power Spectra Plots of $\frac{N_i - N_p}{N_i}$ for MCF's P7, P8, SSP7, and SSP8, Noise Sample C	22
18	Matrix of Measured Noise Correlations for Single High-Noise Sample	30
19	Frequency Response of Prewhitening and Antialiasing Filter	32
20	Time-Domain Operators for 10-Channel, 27-Point Filter, Developed from a Single High-Noise Sample	33
21	Time-Domain Operators for MCF-11, 27 Point Filter	34
22	Amplitude Response of MCF-11	35
23	Resampled High-Noise Sample with Prediction Estimate Simple Summation and Filtered Traces (High-Noise Filter)	37

LIST OF ILLUSTRATIONS

Figure	Description	Page
24	Signal-To-Noise Improvement Curves Comparing Filtered, Summed and Reference Data	38
25	High-Noise Sample With Actual Signal Added	40
26	Noise Rejection Using "Road Noise" Filter	41
27	Resampled High-Noise Sample with Prediction Estimate, Prediction Error, Simple Summation, and Filtered Traces (MCF-11)	43
28	Resampled Normal-Noise Sample with Prediction Estimate, Prediction Error, Simple Summation, and Filtered Traces (MCF-11)	44
29	Signal-To-Noise Improvement Curves for High-Noise Samples Comparing Filtered, Summed and Reference Data	45
30	Signal-To-Noise Improvement Curves for Normal-Noise Sample Comparing Filtered, Summed and Reference Data	46
31	Prediction Error-To-Reference Noise Power Ratios for High-Noise and Normal-Noise Samples	47
32	Random Noise Response for 27-Point MCF with "Road Noise" in Design Ensemble	47
33	Signal Sample Used in Evaluation of the On-Line Processors	49
34	Noise Sample Used in Evaluation of the On-Line Processors	49
35	Signal Data Filtered On-Line Compared with the Same Data Filtered on the IBM 7044	50
36	Noise Data Filtered On-Line Compared with the Same Data Filtered on the IBM 7044	51

SECTION I

INTRODUCTION

A study was conducted to determine the amount of predictable noise at Uinta Basin Seismological Observatory (UBO). A comparison of the surface and the 200-ft buried array was made to determine how much noise was present which attenuated rapidly with depth. Twenty-two noise prediction filters were designed and evaluated for the surface and subsurface array. Each one predicted the output of the center seismometer in the respective arrays.

Two analog multichannel processors were installed at UBO during the latter part of 1965. These are special-purpose analog computers that provide real-time multichannel processing capabilities.

A number of distinct multichannel filters were developed for these processors using the Wiener least-mean-square techniques. Theoretical filter weights were converted to resistor values, and printed circuit filter cards were subsequently fabricated and installed in the on-line processors. These filters were designed for the particular array geometries present at UBO. The 10-channel processor is operating on data from a 10-element surface array. The 19-channel processor is operating on data from a 10-element subsurface array and a 6-element vertical line array installed in a deep well near the center of the 10-element arrays.

Certain side effects were introducted as a result of the signal and noise statistics used in developing the multichannel filters. Locally-generated, fundamental-mode Rayleigh energy appeared as a signal on the surface array and was passed, rather than rejected, by the processor. The output was contaminated, and overall signal-to-noise improvement was reduced as a result of these spurious "signals".

Once this problem was recognized, an attempt was made to classify the particular energy in question and determine the effectiveness of multichannel processing. New filters were developed and installed on-line. Preliminary indications are that no significant overall improvement has resulted.

A limited visual analysis was made of the effectiveness of the on-line processors. This was effected by comparing the on-line processed data with the corresponding data processed on the IBM 7044. In most cases the two sets of processed data were quite similar.

SECTION II

UBO NOISE PREDICTION STUDY

A. SUMMARY

The purpose of this study was to determine the amount of predictable noise at Uinta Basin Seismological Observatory (UBO) by the development and application of noise prediction filters.

A comparison of the surface and the 200-ft buried array was conducted to determine if a large amount of noise was present which attenuates rapidly with depth.

The determination of the amount of predictable noise at a particular array is desirable to determine or to explain the effectiveness of multichannel processing. A measure of the amount of predictable noise at a particular station gives a rough measure of the signal-to-noise improvement possible with multichannel processing above that obtained with straight sum processing. In the presence of random noise, both processes give a maximum signal-to-noise improvement of $\sqrt{N}$ where N is the number of seismometers in the array.

Twenty-two noise prediction filters were designed on, applied to and evaluated for the surface and subsurface planar arrays at UBO. Prediction filters were designed upon the nine outlying individual seismometers in each array and also upon the nine sensors summed into three rings. Each type predicted the output of the center seismometer.

Results of this study indicate that:

- Below 1.25 cps, the noise field at UBO is highly predictable, reaching a peak of approximately 30 db (96-7/8 percent) predictability from 0.25 to 0.50 cps
- Above 1.25 cps, the noise field appears almost random to the UBO planar array with 0 to 3 db (0 to 25 percent) predictability except for an occasional highly predictable noise peak at 2.7 cps which has been shown to be road noise* and two smaller peaks at 5.2 cps and 5.4 cps of 6 db (50 percent) predictability
- Three-channel ring-summed filters are unable to predict the noise peaks, when present, at 2.7, 5.2 and 5.4 cps

*Burrell, George C., 1966: Array Research Semiannual Tech. Rpt. No. 5, Analysis of UBO Road Noise, Sec. VI, AFTAC Project VT/4053, July.

- There is no noticeable difference between the surface- and the subsurface-recorded ambient noise as indicated both by the high degree of predictability of surface data from subsurface data and by the similarity of single noise spectra

From this study of noise prediction filters in relation to the effectiveness of MCF processing it may be concluded that:

- If it were possible to eliminate all of the predictable noise while preserving desired signals at UBO, an absolute maximum of 30-db S/N improvement theoretically could be reached in the frequency region of 0.25 to 0.50 cps
- Above 1.5 cps, MCF processing is limited to 3-db improvement relative to straight-sum processing with the exception of the predictable noise peaks (when present) at 2.7, 5.2 and 5.4 cps where MCF processing should give a maximum of 10 db, 6 db and 6 db improvement, respectively, above straight sum processing
- Based upon the ring-summed filtering results, it would seem that 4-channel ring-summed signal extraction filters would not eliminate road noise at UBO
- The fact that the spectra from the surface and the subsurface array are nearly identical indicates that there was not a great deal of noise (i.e., wind noise) that exponentially attenuates with depth

B. PRESENTATION OF RESULTS

In order to determine the amount of predictable noise at UBO, prediction filters were designed to predict the center seismometer of the surface of subsurface planar array. Computed were power density spectra of the quantity

$$\frac{N_i - N_p}{N_i}$$

where

N_i is the noise input (the output of the center seismometer)

N_p is the predicted output for the center seismometer.

The quantity $\left|\frac{N_i - N_p}{N_i}\right| \times 100\%$ might be aptly termed the "percent unpredictability", since $\left|\frac{N_p}{N_1}\right| \times 100\%$ is the percent predictability.

Table 1 presents the filters which were designed on individual sensors and ring sums. Both single and ensemble noise statistics were used and, additionally, interarray prediction was investigated.

A representation of the seismic arrays at UBO is shown in Figure 1. Two planar arrays, each consisting of 10 vertically responsive velocity seismometers, are represented. One array is located at the surface, and the second is buried at a depth of 200 ft beneath the corresponding surface sensors. Six other vertically responsive instruments are installed to form a vertical line array within a deep well located directly beneath Z6.

Figure 2 shows power density spectra of noise samples A, B and C, respectively. Note that the road noise at 2.7 cps is present only on noise sample B (NSB). This is probably because the noise samples were taken over the weekend. Noise sample A (NSA) was recorded on Saturday, 27 March 1965. NSB and NSC were recorded on Sunday, 28 March 1965. Therefore, intermittent road noise rather than constant road noise would be expected. The wiggly trace outputs of the MCF's and the associated reference and error traces are seen in Figures 3, 5, 7, 10, 12, 14, and 16.

Figures 4a, 4c, 6a, 6c, 8a, and 8c for NSA, Figures 11, 13a and 13c for NSB, and Figures 15, 17a and 17c for NSC show that 9-channel filters are superior for noise prediction and, hence, for noise rejection. In all cases the 9-channel filters do a better overall job of predicting noise throughout the frequency range of interest. In Figures 11, 13a and 13c, the 9-channel filters predict the coherent noise peaks at 2.7, 5.2 and 5.4 cps while the 3-channel filters do not. The 3-channel filters 6a, 6c, 9c, and 15 have evidently misdesigned and the cause of misdesign is not known.

Table 1

FILTER DESIGN PARAMETERS

Prediction Filter	Designed on						No. Channels		Predicts	
	Subsurface	Surface	NSA	NSB	NSC	Σ	9	3	SZ10	Z10
SP1	X		X				X		X	
SP2	X					X	X		X	
SP3	X		X					X	X	
SP4	X					X		X	X	
P1		X	X				X			X
P2		X				X	X			X
P3		X	X					X		X
P4		X				X		X		X
SSP1	X		X				X			X
SSP2	X					X	X			X
SSP3	X		X					X		X
SSP4	X					X		X		X
SP5	X			X			X		X	
SP6	X			X				X	X	
P5		X		X			X			X
P6		X		X				X		X
SSP5	X			X			X			X
SSP6	X			X				X		X
SP7	X				X		X		X	
SP8	X				X			X	X	
P7		X			X		X			X
P8		X			X			X		X
SSP7	X				X		X			X
SSP8	X				X			X		X

Note: Z10 is center seismometer of surface array
SZ10 is center seismometer of subsurface array
S prefix indicates subsurface
SS prefix indicates subsurface to surface

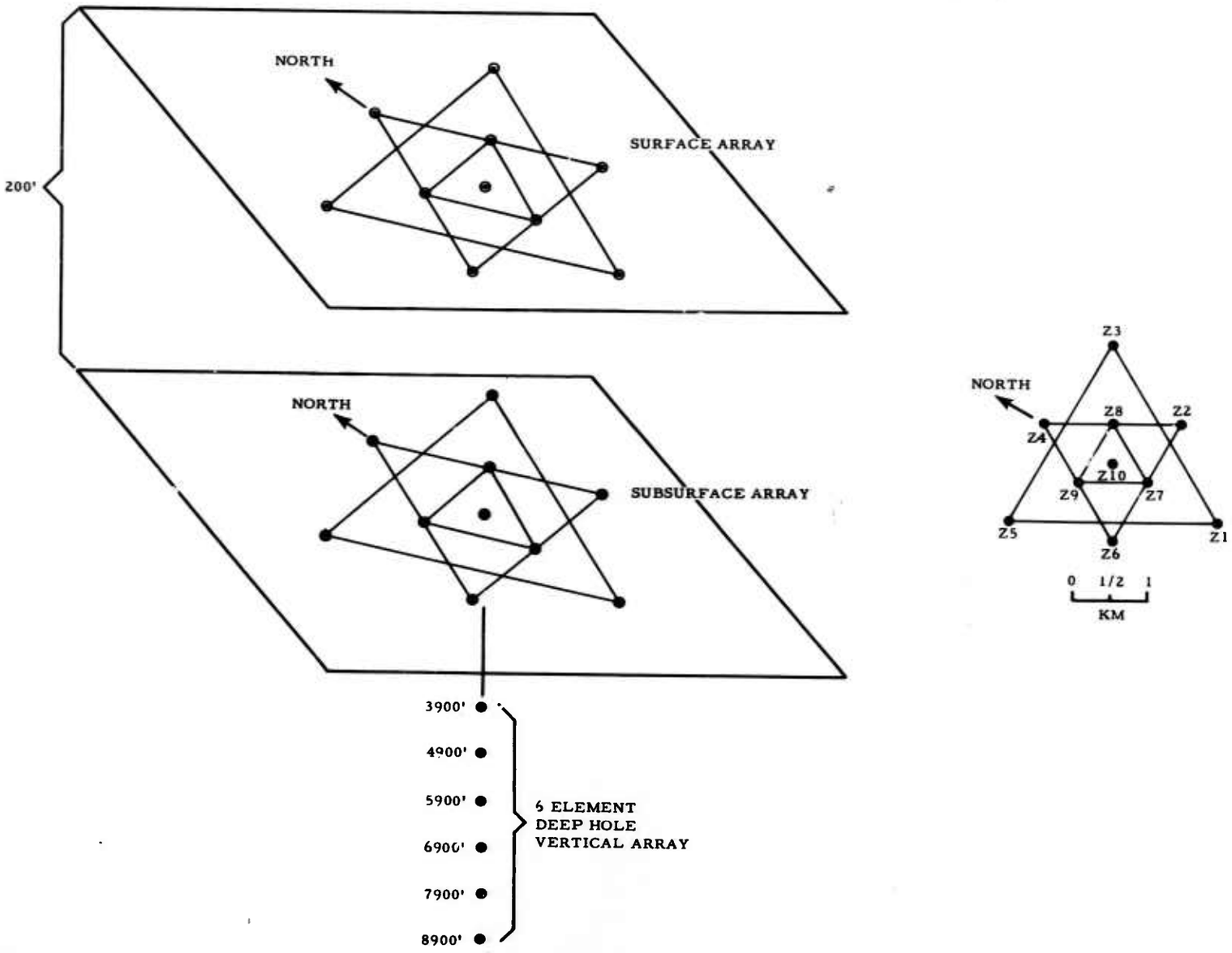

Figure 1. Artist's Concept of UBO Array Complex

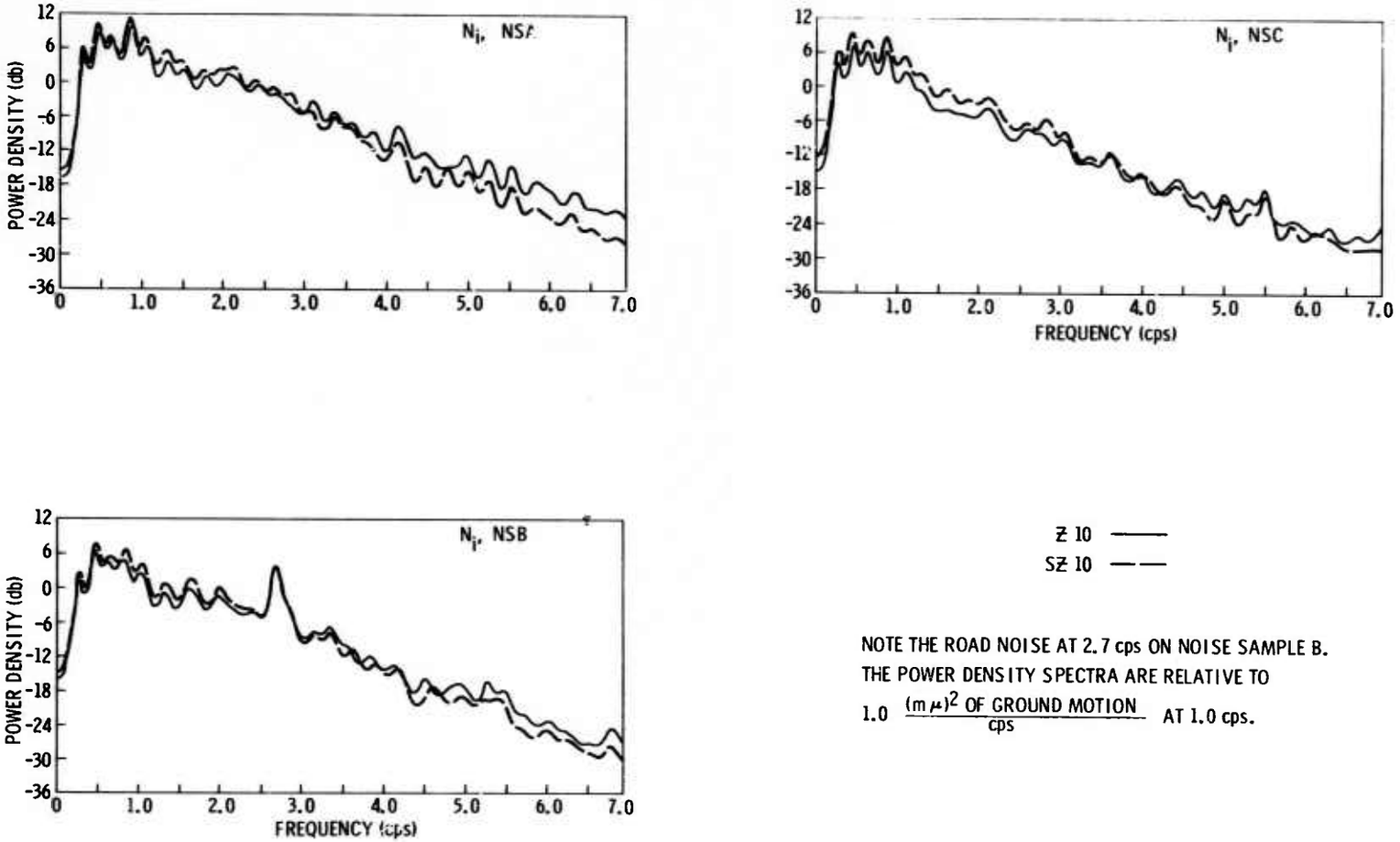

Figure 2. Power Density Spectra of the Center Seismometer for the Surface Array (Z 10) and for the Subsurface Array (SZ 10) for Noise Sample A (NSA), Noise Sample B (NSB) and Noise Sample C (NSC)

science services division

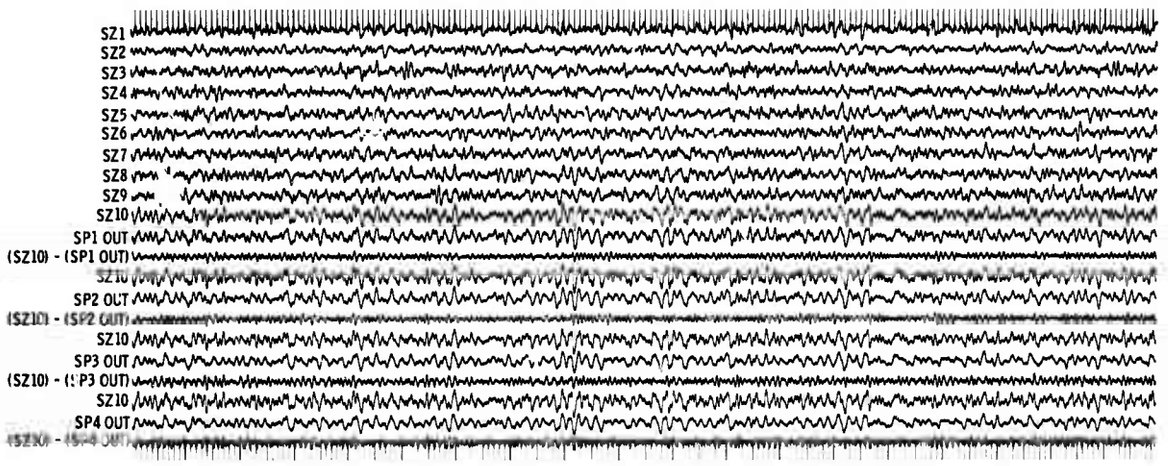

Figure 3a. A Short Portion of NSA Complete With the Output of the MCF's SP1, SP2, SP3, and SP4, and Their Error Traces

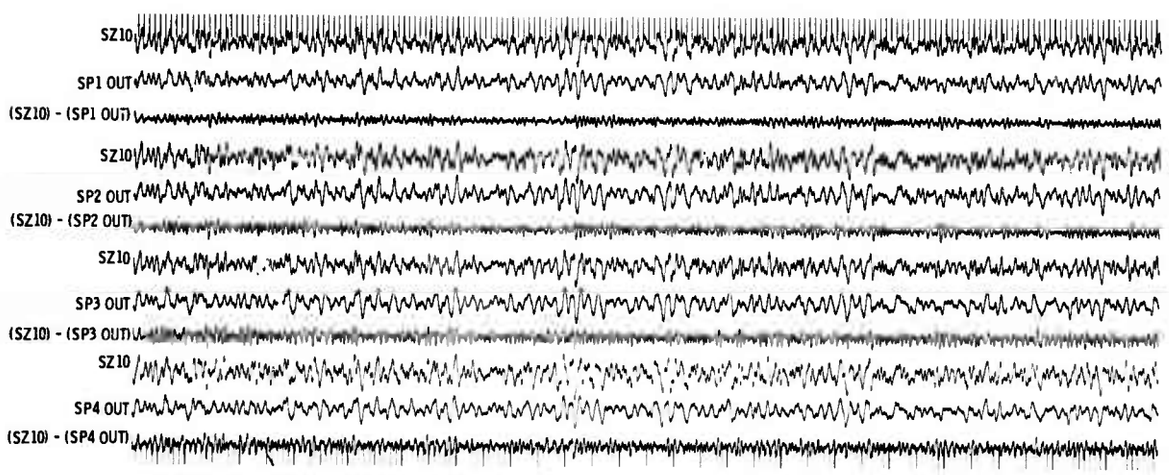

Figure 3b. Enlargement of Traces 10 through 21 in Figure 3a

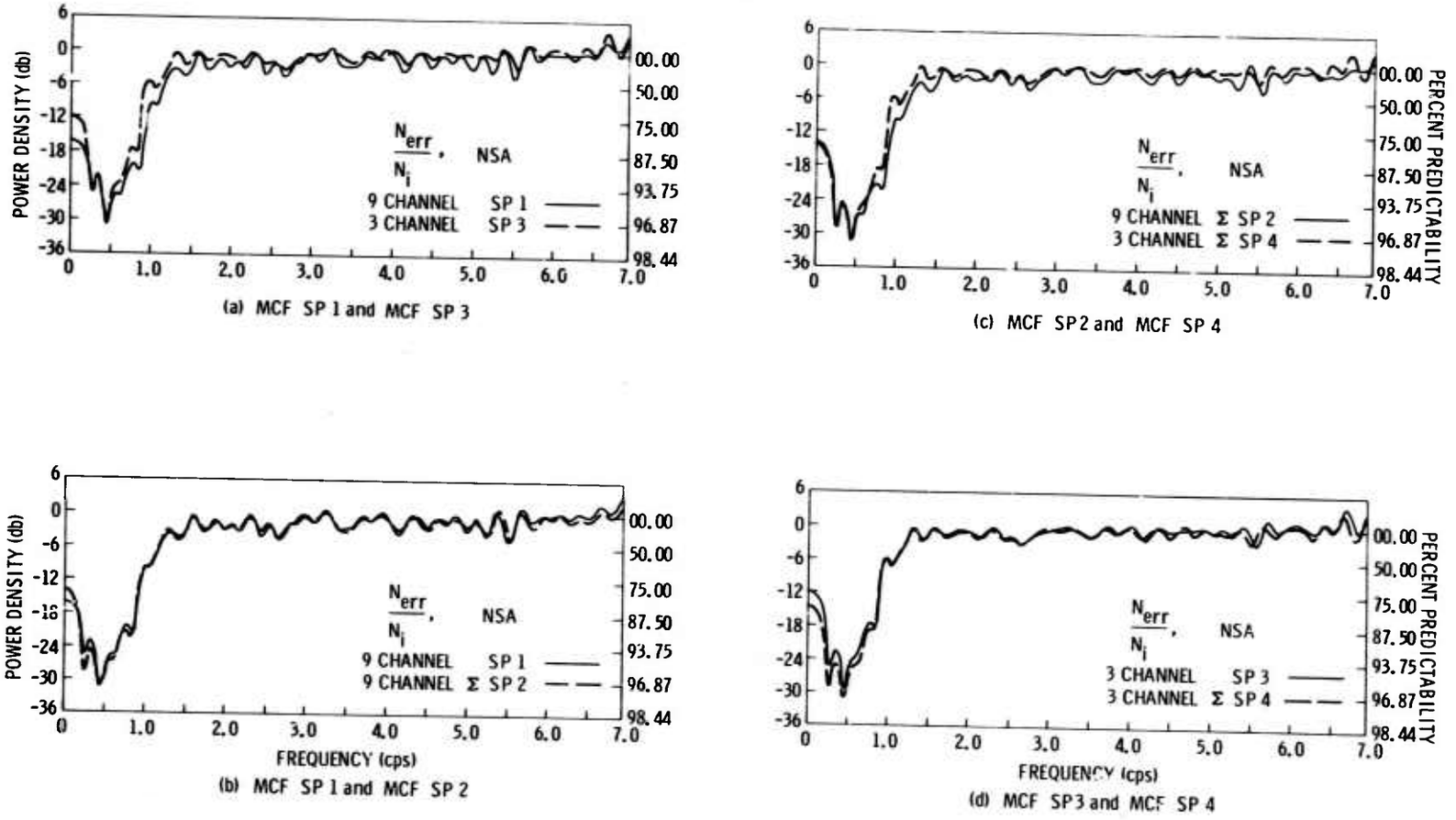

(a) MCF SP 1 and MCF SP 3

(c) MCF SP 2 and MCF SP 4

(b) MCF SP 1 and MCF SP 2

(d) MCF SP 3 and MCF SP 4

Figure 4. Power Spectra Plots of $\frac{N_i - N_p}{N_i}$ for MCF's SP1, SP2, SP3 and SP4, Noise Sample A

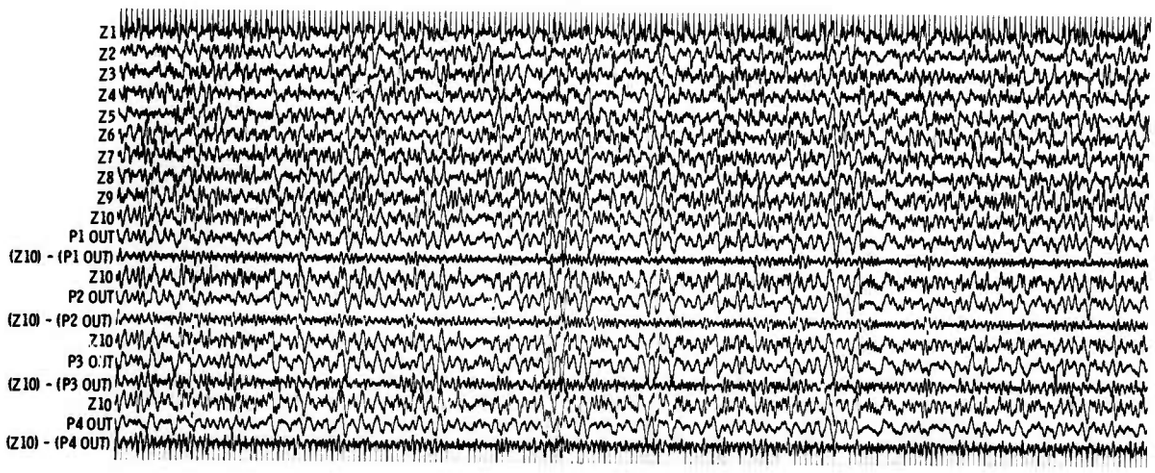

Figure 5a. A Short Portion of NSA Traces 10 through 21 are the Reference Trace Z 10, the Predicted Traces and the Error Traces for MCF's P1, P2, P3 and P4

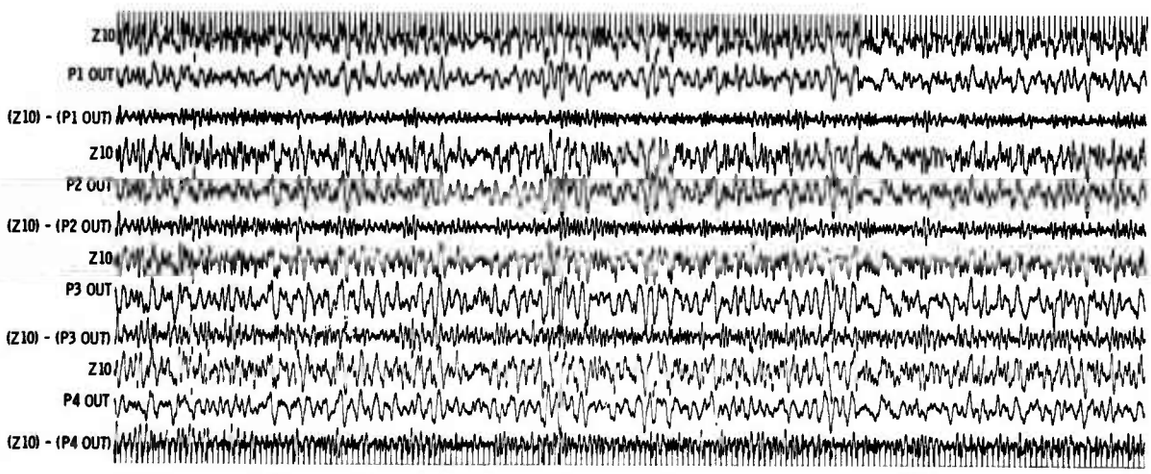

Figure 5b. Enlargement of Traces 10 Through 21 in Figure 5a

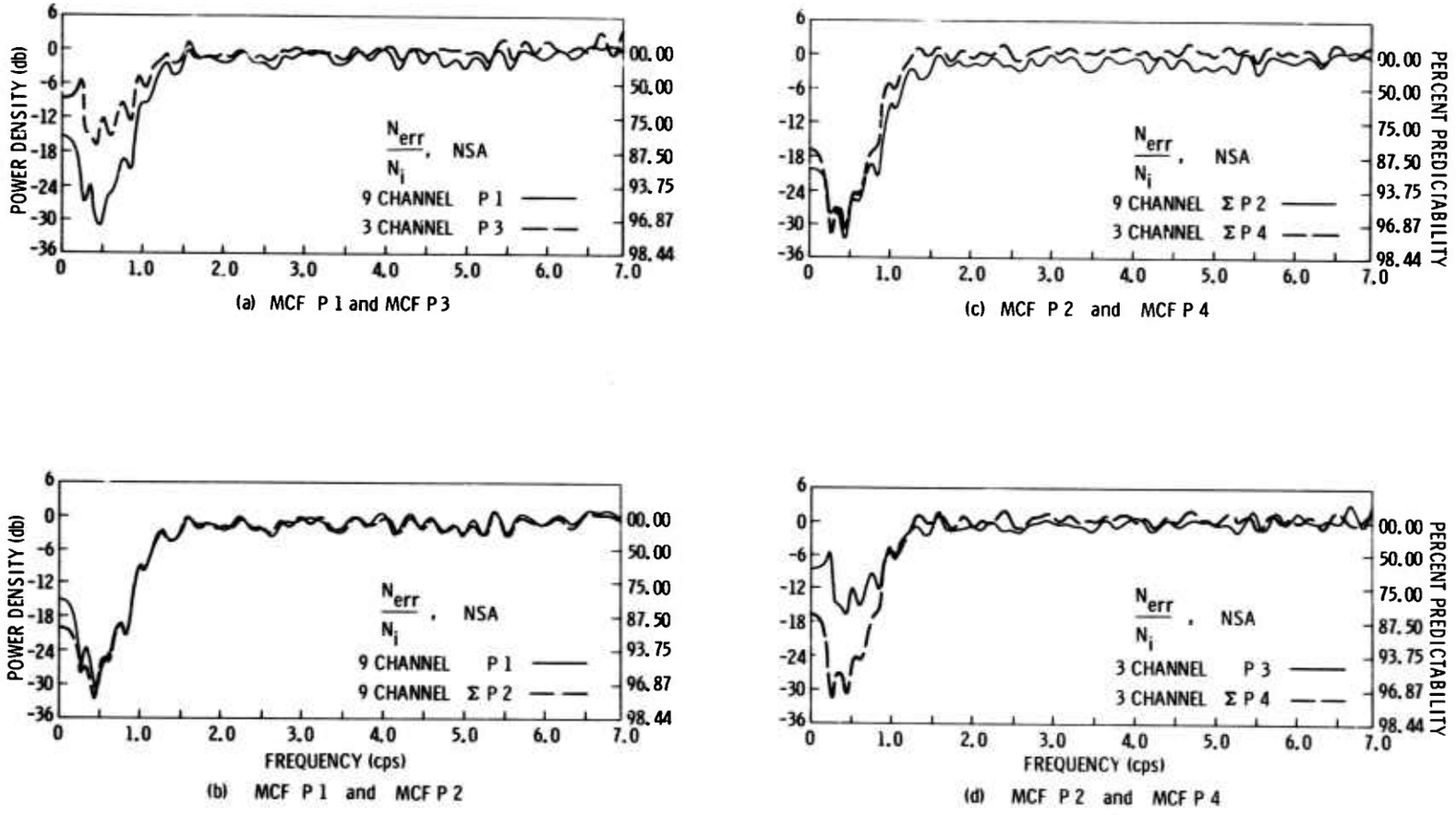

(a) MCF P 1 and MCF P 3

(c) MCF P 2 and MCF P 4

(b) MCF P 1 and MCF P 2

(d) MCF P 2 and MCF P 4

Figure 6. Power Spectra Plots of $\frac{N_i - N_p}{N_i}$ for MCF's P1, P2, P3 and P4, Noise Sample A

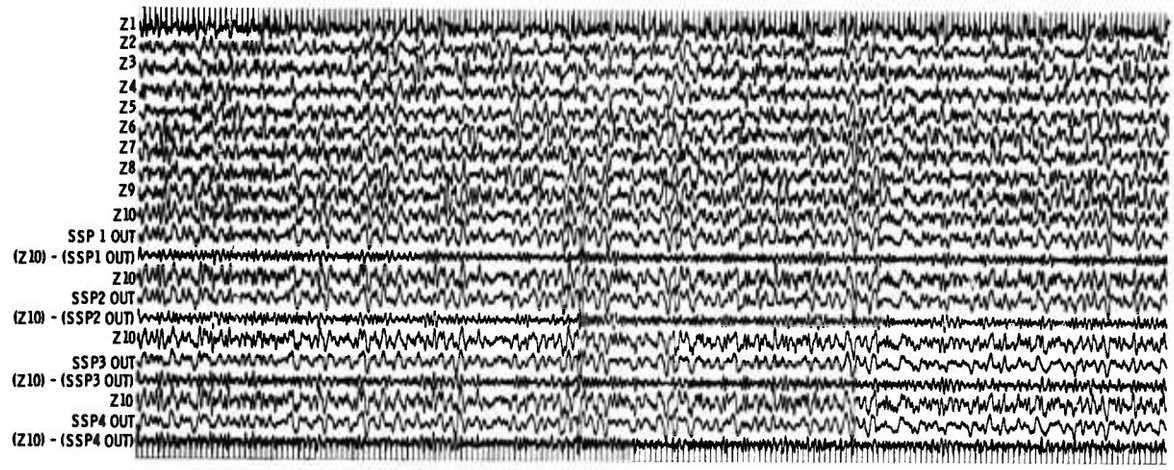

Figure 7a. A Short Portion of NSA, With the Output of the MCF's SSP1 through SSP4, and Error and Error and Reference Traces

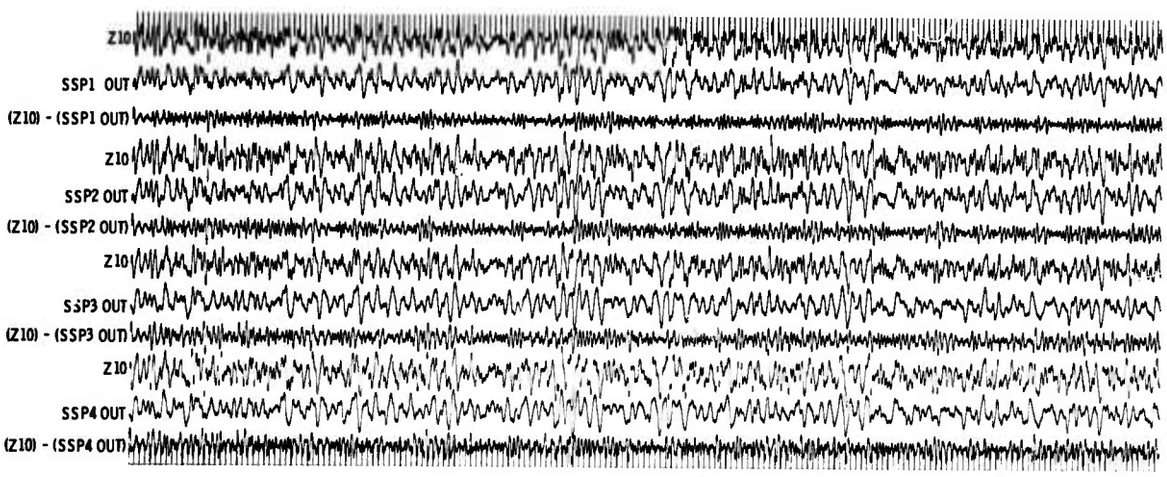

Figure 7b. Enlargement of Traces 10 through 21 in Figure 7a

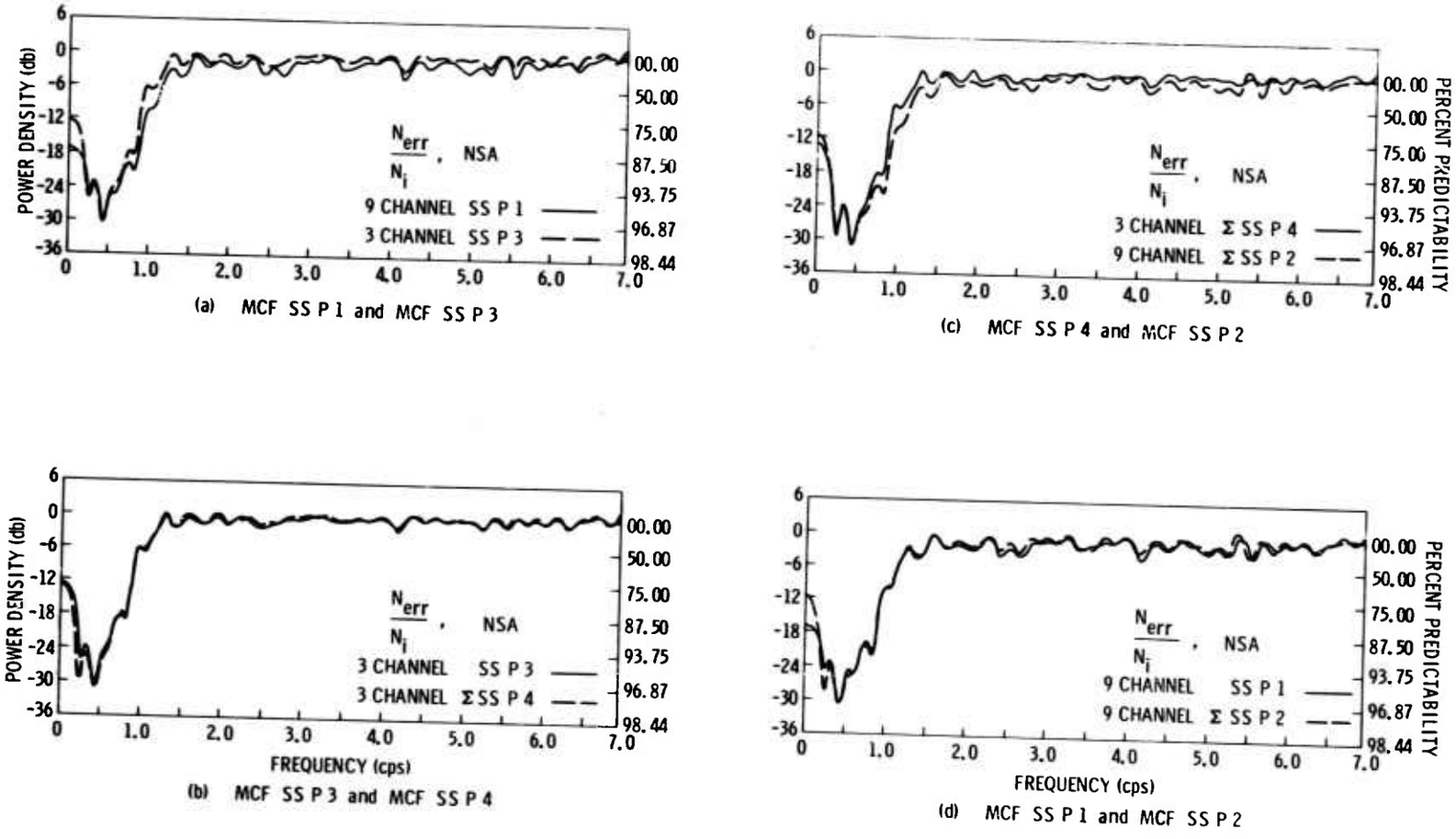

Figure 8. Power Spectra Plots of $\frac{N_i - N_p}{N_i}$ for MCF's SSP1, SSP2, SSP3, and SSP4, Noise Sample A

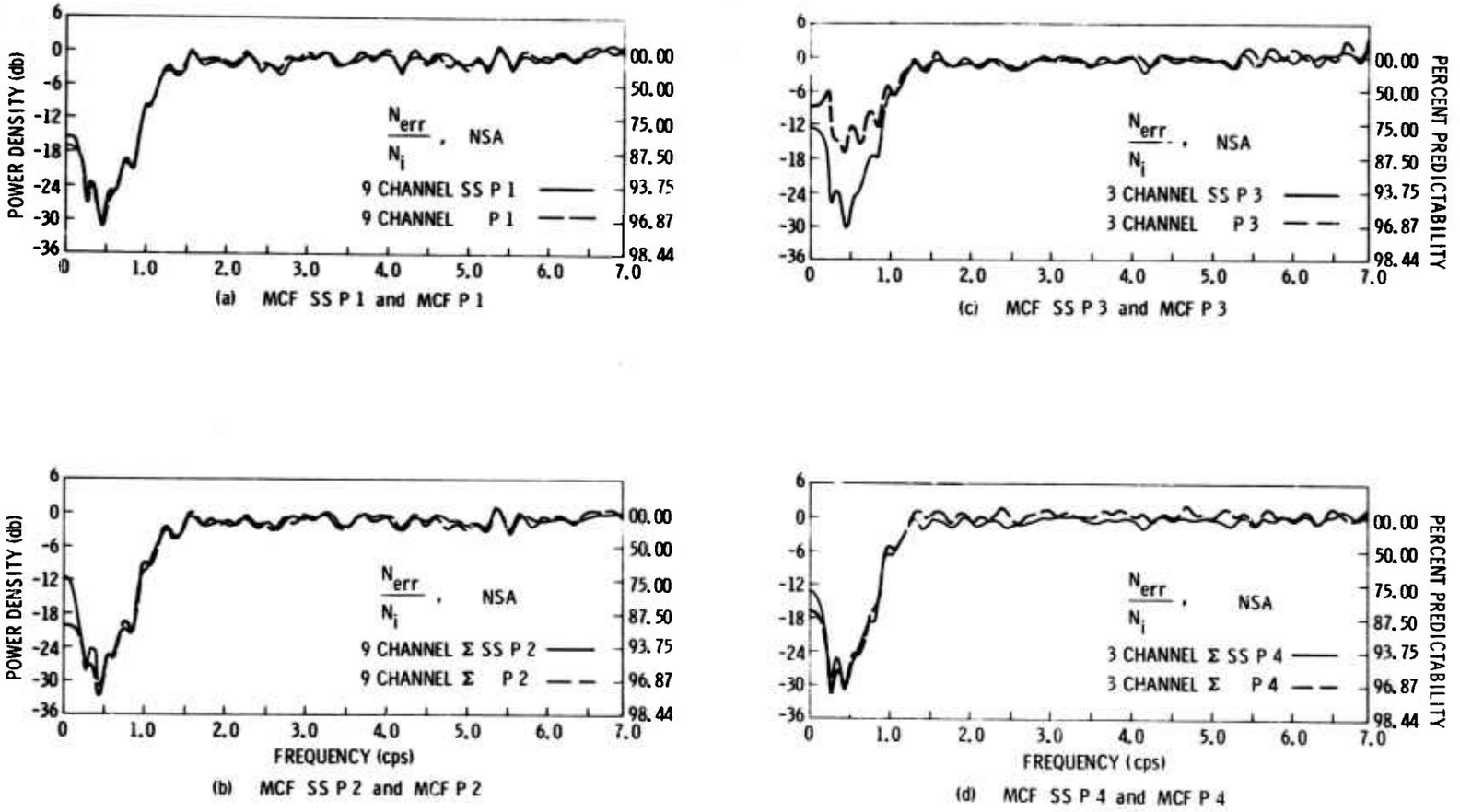

Figure 9. Power Spectra Plots of $\frac{N_i - N_p}{N_i}$ for MCF's P1, P2, P3, P4, SSP1, SSP2, SSP3, and SSP4, Noise Sample A

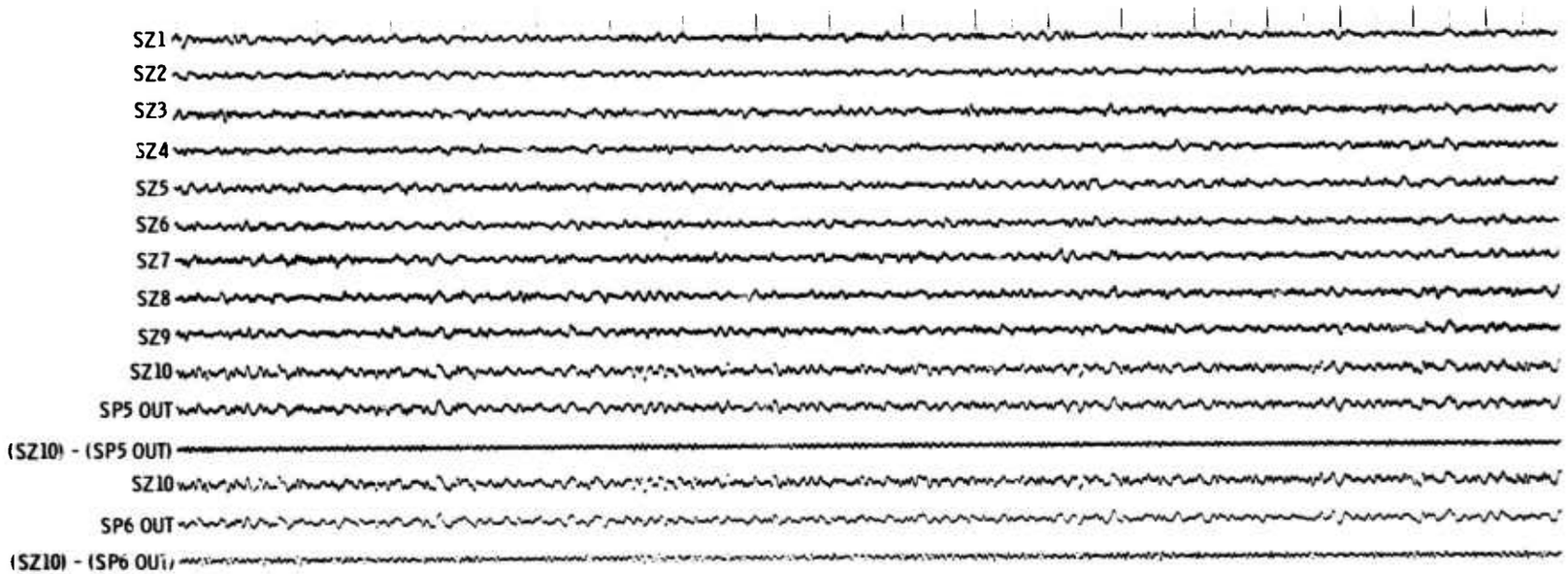

Figure 10. A Short Portion of Subsurface NSB, With the Outputs of MCF's SP5 and SP6, Reference Traces (SZ 10), and Error Traces

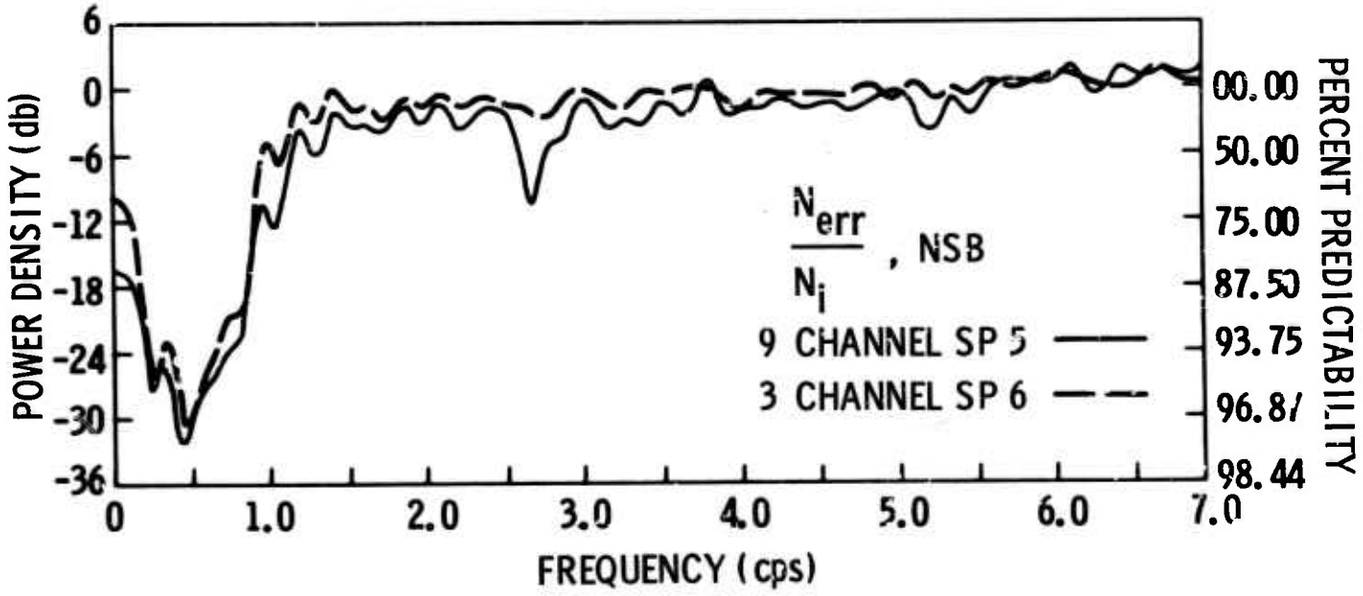

Figure 11. Power Spectra Plots of $\frac{N_i - N_p}{N_i}$ for MCF's SP5 and SP6, Noise Sample B

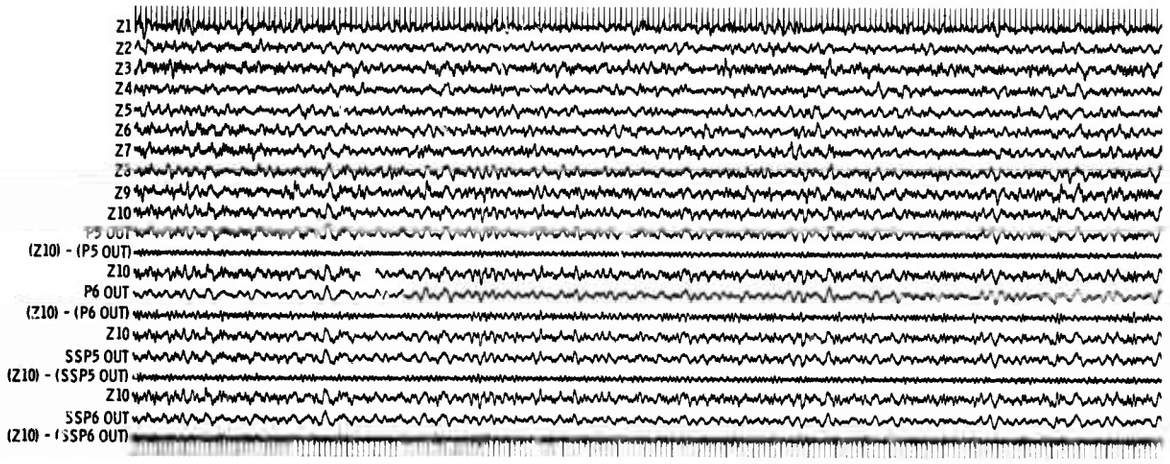

Figure 12a. A Short Portion of NSB (Surface), with the Output of MCF's P5, P6, SSP5, and SSP6, Reference Traces and Error Traces

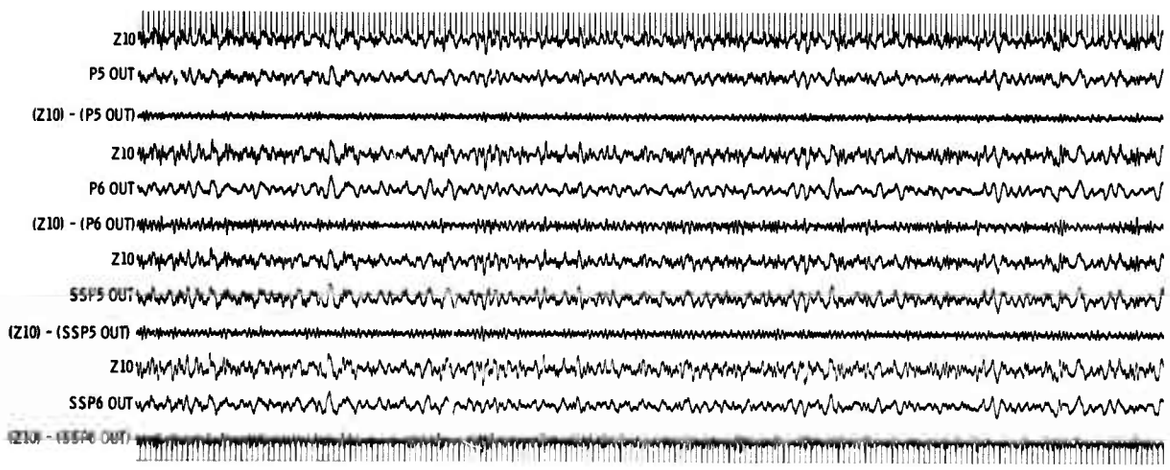

Figure 12b. Enlargement of Traces 10 Through 21 in Figure 12a

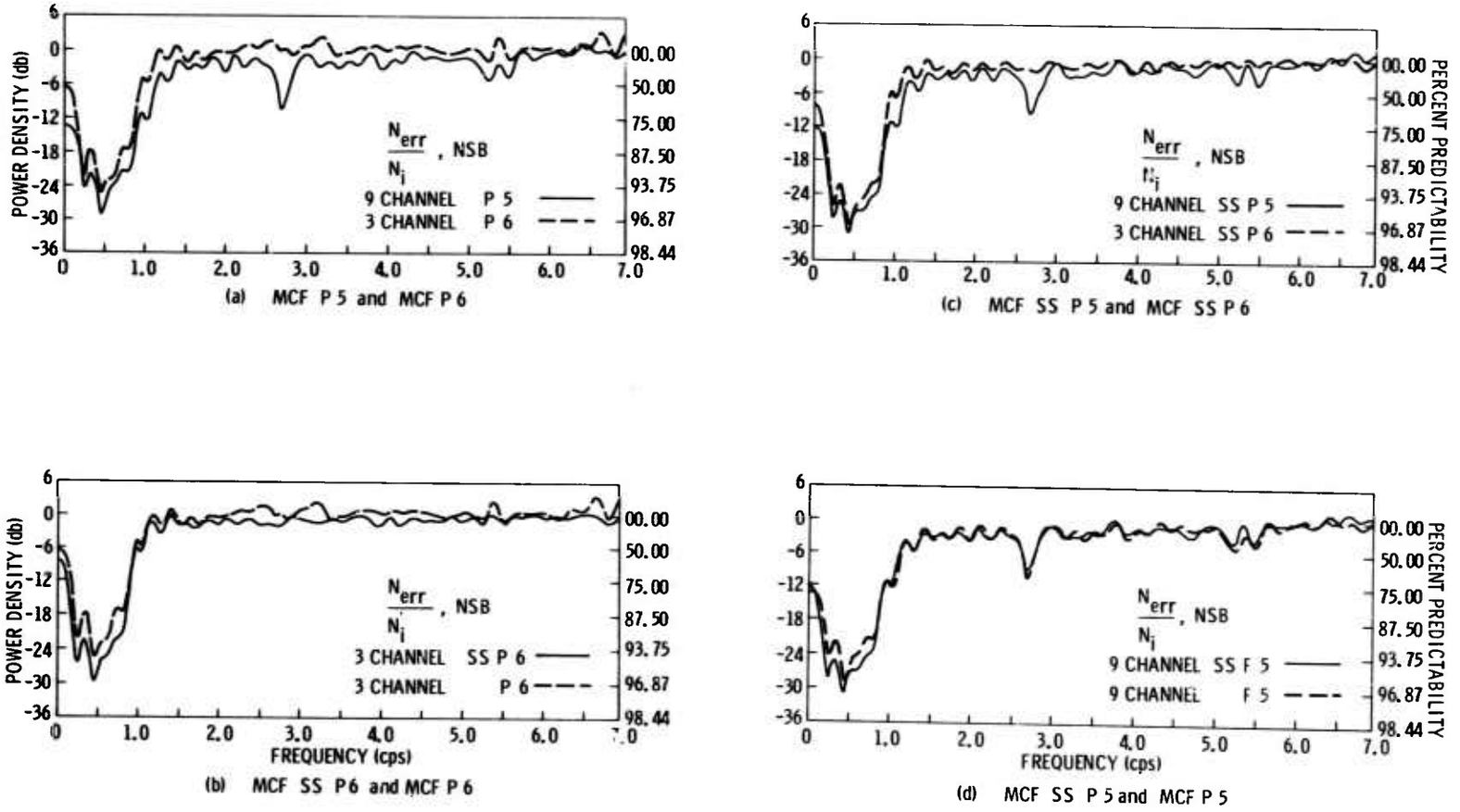

Figure 13. Power Spectra Plots of $\frac{N_i - N_p}{N_i}$ for MCF's P5, P6, SSP5, and SSP6, Noise Sample B

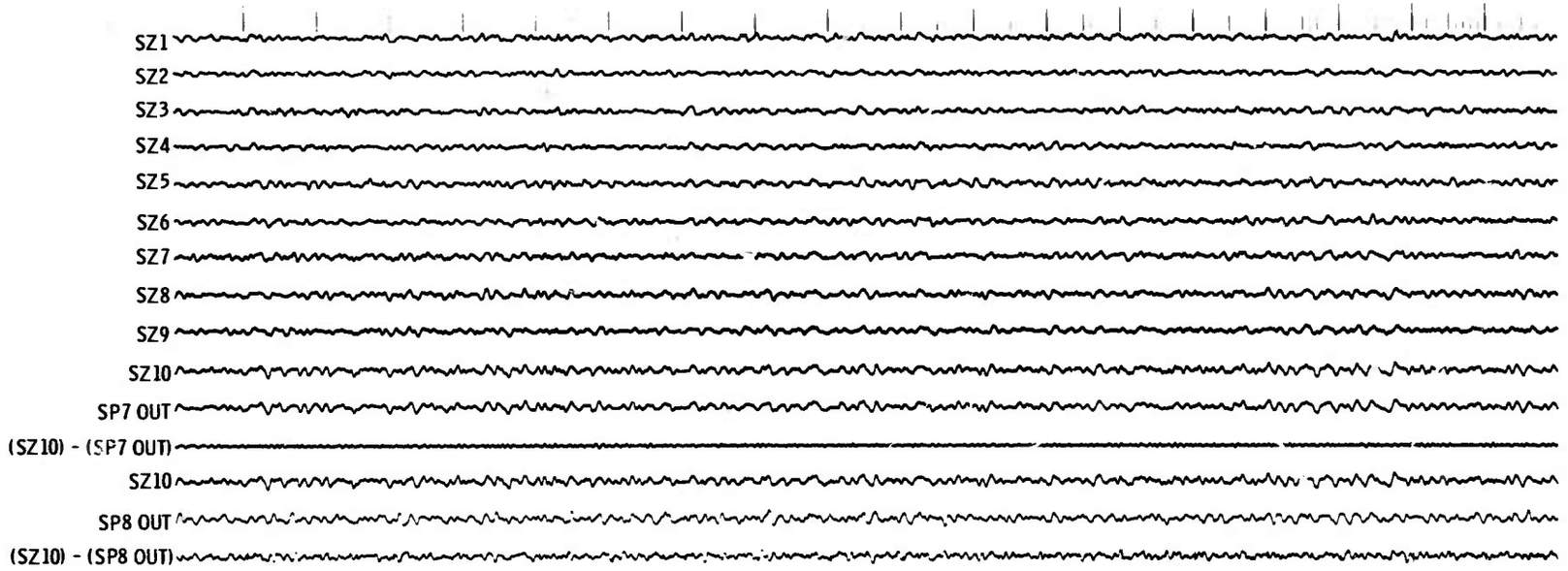

Figure 14. A Short Portion of NSC (Subsurface) With the Output of MCF's SP7 and SP8, Reference Traces, and Error Traces

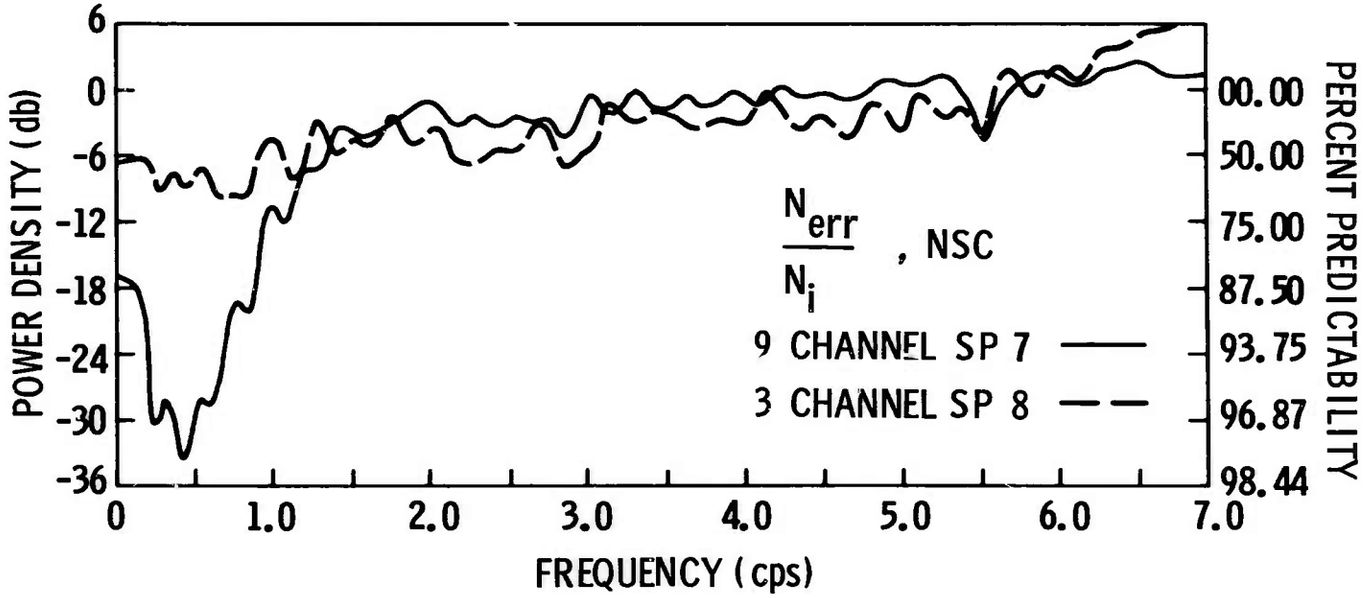

Figure 15. Power Spectra Plots of $\frac{N_i - N_p}{N_i}$ for MCF's SP7 and SP8, Noise Sample C

Figure 16a. A Short Portion of NSC (Surface) with the Outputs of MCF's P7, P8, SSP7, SSP8, Reference Traces, and Error Traces

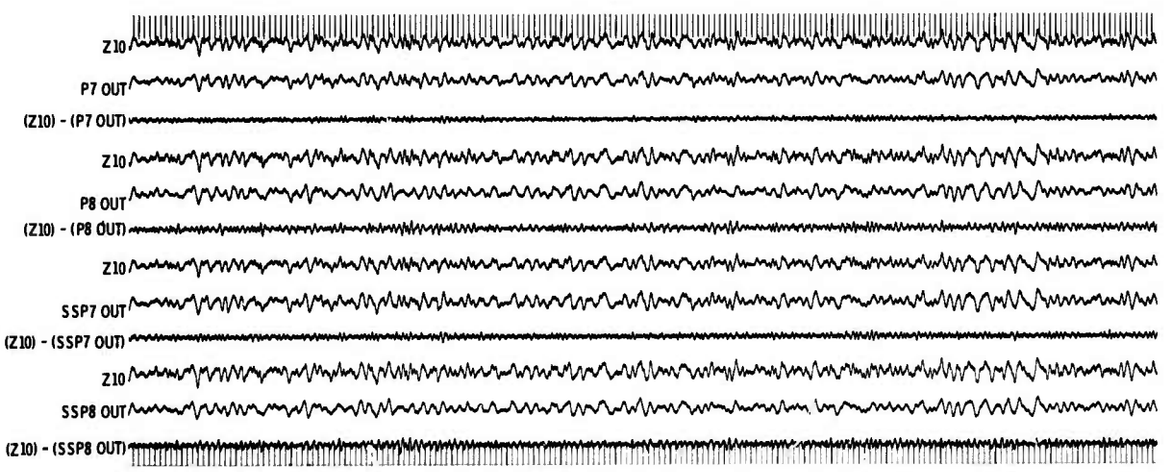

Figure 16 b. Enlargement of Traces 10 Through 21 in Figure 12a

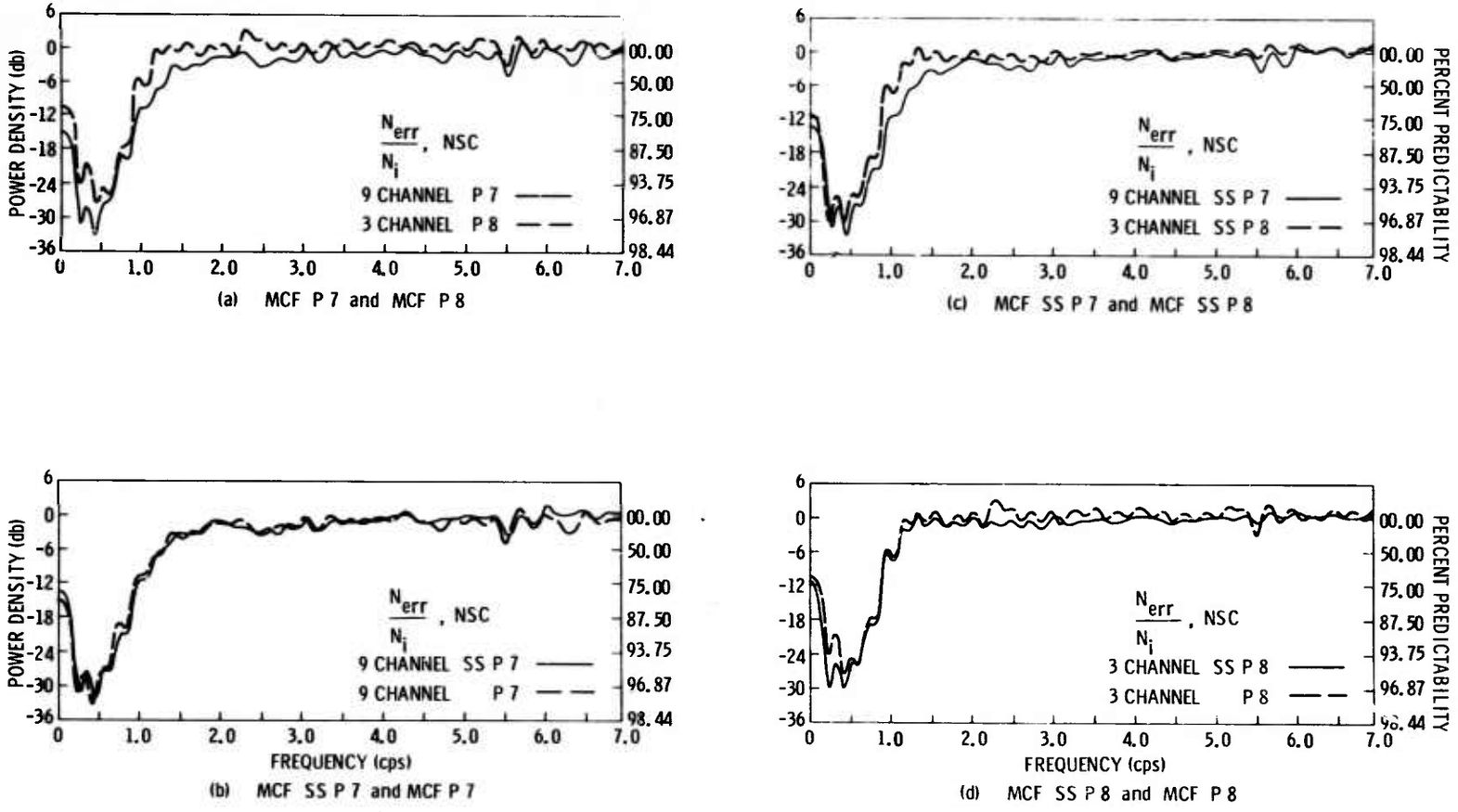

Figure 17. Power Spectra Plots of $\frac{N_i - N_p}{N_i}$ for MCF's P7, P8, SSP7, and SSP8, Noise Sample C

Figures 4b, 4d, 6b, 8b, and 8d show that filters designed upon the sum of NSA, NSB and NSC perform as well as those designed upon the individual NSA. Filters designed on the sum of the noise samples appear to predict approximately 3-db better at 0.25 cps than ones designed individually on NSA. This might be explainable in terms of the accuracy of the power spectrum estimate program which was used to calculate the spectra. The fact that filters designed on the subsurface array do as well as the filters designed on the surface array in predicting the surface center seismometer is shown in Figure 9 for NSA, in Figures 13b and 13d for NSB, and in Figure 17b and 17d for NSC.

The fact that the filters designed on the ensemble of NSA, NSB and NSC perform as well as the filters designed on NSA would seem to indicate that the noise statistics remained time-stationary during the 2-day period covered by the noise recordings. Since the subsurface is as able to predict the center surface seismometer output as well as the surface array, the degree of predictable noise coherence between the surface and subsurface array is indicated to be quite large.

Results of this study show that:

- If it were possible to eliminate all predictable noise at UBO while preserving the desired signal, an absolute maximum of 30 db S/N improvement theoretically could be reached in the frequency region of 0.25 to 0.50 cps. However, it has been guessed* that in this frequency band a large portion (15 to 20 percent) of the observed noise power at UBO consists of mantle P-wave noise which overlaps the desired teleseismic signal in f-$\vec{k}$ space. Hence, maximum S/N improvement above a single seismometer should be limited to approximately 7 to 8 db.
- Above 1.5 cps, MCF processing is limited to 3db improvement relative to straight sum processing, with the exception of the predictable noise peaks at 2.7, 5.2 and 5.4 cps where MCF processing should give a maximum of 10 db, 6db improvement, respectively, above straight sum processing.
- Based upon the ring-summed prediction filtering results, 4-channel ring-summed signal extraction filters would not eliminate road noise at UBO.

*Texas Instruments Incorporated, 1965: Array Research Semiannual No. 3, Contract AF33(657)-12747, Section I, 3 Jun.

- The large amount of coherence between the surface and the subsurface array indicates that, during the time interval of noise samples A, B and C, there was not too much noise attenuating rapidly with depth.

Ibid

SECTION III

ANALOG PROCESSORS AT UBO

Theory developed during early studies at Texas Instruments indicated the feasibility of increasing the signal-to-noise ratio of earthquake and explosion signals by multichannel filtering in 3-dimensional frequency-wavenumber ($f\text{-}\vec{k}$) space. A prototype Multiple Array Processor (MAP) was subsequently constructed to incorporate multichannel processing in real-time hardware. Second-generation analog MAP systems were constructed to provide additional flexibility and facility of operation. Two of these systems were installed in September 1965, and are presently operating on-line at the UBO array

A. MULTICHANNEL PROCESSORS AT UBO

The two processors installed at UBO are, in reality, special-purpose analog computers designed to accomplish multichannel filtering on-line in real time. Each processor was programmed to accept raw data as input from the seismic arrays as follows:

- 19-channel system — accepts data from the 10-element subsurface planar array and 6-element vertical deep-well array
- 10-channel system — accepts data from the 10-element surface planar array

Based upon seismic signal and ambient noise statistics recorded previously at UBO, a number of distinct theoretical multichannel filters were developed. Theoretical filter weights were then converted to resistor values using the following equation:

$$R(\tau) = \frac{1}{A(\tau)} * SF$$

where

$R(\tau)$ = resistor values

$A(\tau)$ = filter weights

SF = scale factor chosen to cause all resistor values to fall in the range $10K \leq R(\tau) \leq 10M$.

The $R(\tau)$ values were compared with a Military Standard table of available 1 percent resistor values and the nearest value was chosen. The 1 percent limitation on resistor values restricted the effective dynamic range of the resulting filters to something less than 40 db. Resistor cards were fabricated and installed in the processors as the analog equivalent of the theoretical filters.*

B. FILTER DESIGN AND DESIGNATION

A listing of all the various filters developed for the UBO processors is given in Table 2 and Table 3. The various parameters common to each filter are also listed. Included are optimum and beam-steer filters and those filters which were developed but were not installed in the operational MAP.

*A more complete discussion of the analog processors is given in Texas Instruments Incorporated, 1965: Multiple Array Processor, Final Rpt., Contract AF #33(657)-13904, 29 Oct.

Table 2

10-CHANNEL MAP FILTERS (SURFACE ARRAY)

IDENTIFICATION	MAP OUTPUT CHANNELS	INPUT CHANNELS	FILTER TYPE	SIGNAL MODEL	NOISE MODEL	MAP DELAY FOR IMPULSE SIGNAL
UBO MCF-1	1	Z1-10	Optimum	Infinite Velocity S(f)/N(f) = 4.0	Measured Ambient Noise	1.0 sec Relative to Z-10
UBO MCF-2	2	Z1-10	Optimum	Infinite Velocity S(f)/N(f) = 2.75 f ≥ 1.0 cps For f < 1.0 cps S(f) Decreases at Approximately 18-db/octave	Measured Ambient Noise	1.0 sec Relative to Z-10
UBO MCF-3	3	Z1-10	Optimum	Infinite Velocity to 8.1 KM/sec, S(f)/N(f) = 4.0	Measured Ambient Noise	1.0 sec Relative to Z-10
UBO BS-1	4	Z1-10	Beam Steer	8.1 KM/sec 0° From N	N/A	1.0 sec Relative to Z-10
UBO BS-2	5	Z1-10	Beam Steer	8.1 KM/sec 60°E From N	N/A	1.0 sec Relative to Z-10
UBO BS-3	6	Z1-10	Beam Steer	8.1 KM/sec 120°E From N	N/A	1.0 sec Relative to Z-10
UBO BS-4	7	Z1-10	Beam Steer	8.1 KM/sec 180°E From N	N/A	1.0 sec Relative to Z-10
UBO BS-5	8	Z1-10	Beam Steer	8.1 KM/sec 240°E From N	N/A	1.0 sec Relative to Z-10
UBO BS-6	9	Z1-10	Beam Steer	8.1 KM/sec 300°E From N	N/A	1.0 sec Relative to Z-10
UBO SS-1	10	Z1-10	Straight Sum.	Infinite Velocity	N/A	1.0 sec Relative to Z-10
UBO MCF-4*	N/A	Z1-10	Optimum	Isotropic 15.0 to 8.1 KM/sec (S(f)/N(f) = 4.0	Measured Ambient Noise	N/A
UBO MCF-5*	N/A	Z1-10	Optimum	Isotropic 8.1 to 6.0 KM/sec S(f)/N(f) = 4.0	Measured Ambient Noise	N/A
UBO MCF-6*	N/A	Z1-10	Optimum	Infinite Velocity with Gain Fluctuation Added to Signal Model S(f)/N(f) = 4.0	Measured Ambient Noise	N/A
UBO MCF-7*	N/A	Z1-10	Optimum	Infinite Velocity to 8.1 KM/sec with Gain Fluctuation Added to Signal Model S(f)/N(f) = 4.0	Measured Ambient Noise	N/A

*Developed but not installed in MAP.

Table 3

19-CHANNEL MAP FILTERS (SUB-SURFACE ARRAY)

IDENTIFICATION	MAP OUTPUT CHANNELS	INPUT CHANNELS	FILTER TYPE	SIGNAL MODEL	NOISE MODEL	MAP RELAY FOR IMPULSE SIGNAL
UBO MCF-8	1	SZ1-10	Optimum	Infinite Velocity S(f)/N(f) = 4.0	Measured Ambient Noise	1.0 sec Relative to SZ-10
UBO IP-1	2	SZ1-10 on 4 Rings and 6 Vertical	Optimum	Infinite Velocity S(f)/N(f) = 4.0	Theoretical Isotropic Surface-Mode Noise	1.0 sec Relative to SZ-10
UBO IP-2	3	6 Vertical	Optimum	Infinite Velocity S(f)/N(f) = 4.0	Theoretical Isotropic Surface-Mode Noise	1.0 sec Relative to SZ-10
UBO DG-1	4	3 Vertical (4900, 6900, 8900 ft)	Optimum Deghost	Up-Traveling Infinite Velocity S(f)/N(f) = 4.0	Theoretical Isotropic Surface-Mode Noise and Down-Traveling Infinite Velocity Signal	1.55 sec Relative to SZ-10
UBO DG-2	5	3 Vertical (4900, 6900, 8900 ft)	Optimum Deghost	Down-Traveling Infinite Velocity S(f)/N(f) = 4.0	Theoretical Isotropic Surface-Mode Noise and Up-Traveling Infinite Velocity Signal	0.45 sec Relative to SZ-10
UBO DG-3	6	3 Vertical (3900, 5900, 7900 ft)	Optimum Deghost	Up-Traveling Infinite Velocity S(f)/N(f) = 4.0	Theoretical Isotropic Surface-Mode Noise and Down-traveling Infinite Velocity Signal	1.55 sec Relative to SZ-10
UBO DG-4	7	3 Vertical (3900, 5900, 7900 ft)	Optimum Deghost	Down-Traveling Infinite Velocity S(f)/N(f) = 4.0	Theoretical Isotropic Surface-Mode Noise and Up-Traveling Infinite Velocity Signal	0.45 sec Relative to SZ-10
UBO BS-7	8	6 Vertical	Beam Steer	Uptraveling Infinite Velocity P-Waves	N/A	1.55 sec Relative to SZ-10
UBO BS-8	9	6 Vertical	Beam Steer	Up-Traveling 8-KM/sec P-Waves	N/A	1.55 sec Relative to SZ-10
UBO BS-9	10	6 Vertical	Beam Steer	Up-Traveling 8-KM/sec S-Waves	N/A	1.55 sec Relative to SZ-10
UBO BS-10	11	6 Vertical	Beam Steer	Down-Traveling Infinite Velocity P-Waves	N/A	0.45 sec Relative to SZ-10
UBO BS-11	12	6 Vertical	Beam Steer	Down-Traveling 8-KM/sec P-Waves	N/A	0.45 sec Relative to SZ-10
UBO BS-12	13	6 Vertical	Beam Steer	Down-Traveling 8-KM/sec S-Waves	N/A	0.45 sec Relative to SZ-10
UBO SS-2	14	6 Vertical	Straight Sum.	N/A	N/A	N/A

NOTE: All velocities refer to apparent horizontal velocity.

SECTION IV

ROAD NOISE FILTER DESIGN AND IMPLEMENTATION PROBLEMS

A few problem areas were uncovered when the original filters were installed in the two processors at UBO. First, it became obvious that the theoretical filters designed as MCF-8, having a dynamic range in excess of 40 db, were not being represented accurately in analog form. This was a result of the previously mentioned limitations imposed by 1 percent components (1 percent is the equivalent of 40 db). System noise was being introduced and contamination of filtered data resulted.

A second major problem area developed when certain fundamental mode Rayleigh energy impinged on the surface array. This energy proved exceptionally bothersome when filtered by MCF-1. The remainder of this section will be concerned with the investigation and rejection of this noise.

A. UBO ROAD NOISE

Discussion with personnel at UBO revealed that the Rayleigh energy in question is probably originating along a major highway passing within a few miles of the northwest extent of the array. To distinguish this particular energy from other ambient seismic noise it has been labeled "road noise".

Investigation showed that this road noise does not fit the usual description of signal and noise. It does not arrive as a plane wavefront, it attenuates rapidly across the array and it is time varying. For these reasons, conventional $f\text{-}\vec{k}$ representations are unrealistic, and filtering in 3-dimensional $f\text{-}\vec{k}$ space could prove unsatisfactory.

However, an analysis of the coherence of this noise indicated that conventional filtering would be applicable. Although the energy was definitely attenuating across the array, correlation between individual sensors was quite good. Figure 18 presents a complete correlation set for a noise sample containing a significant amount of road noise. Correlation between the various sensors is obvious. Due to aliasing in $f\text{-}\vec{k}$ space, this noise appeared as signal to the processor and therefore was passed instead of rejected. This made the interpretation of output data quite difficult.

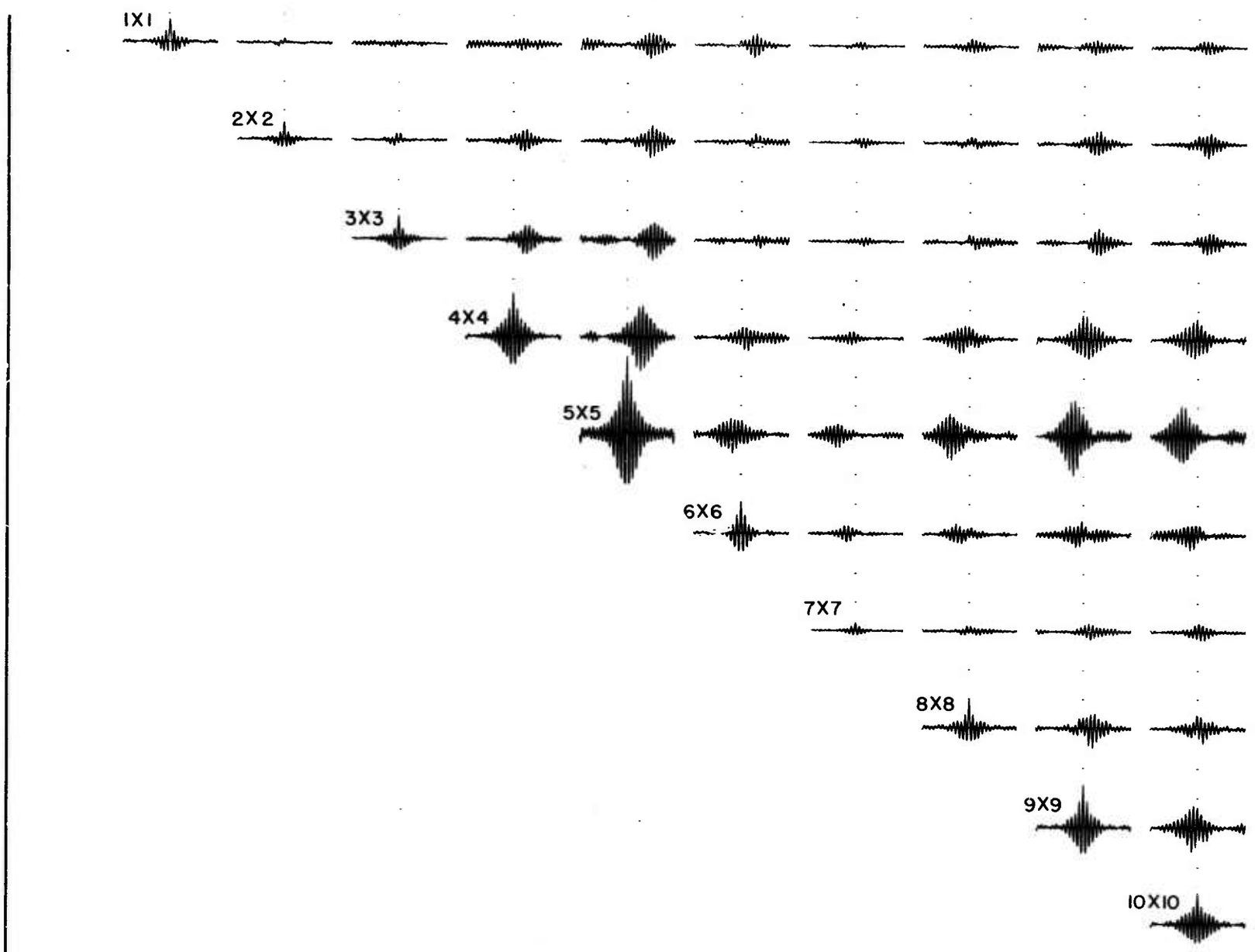

Figure 18. Matrix of Measured Noise Correlations for Single High-Noise Sample.

B. SYNTHESIS OF ROAD NOISE FILTERS

In an attempt to reject this particular energy while preserving the signals, two sets of filters were designed using techniques similar to those described for MCF-1.* The first set was designed using the single 2-min noise sample containing road noise. The second set combined this high-noise sample with four "normal" samples in the design ensemble.

1. High-Noise Filter

Initially, a 27-point multichannel filter was developed from and applied to the high-noise sample after the sample had been resampled by three and filtered with the antialiasing, prewhitening filter displayed in Figure 19. The autocorrelation of the noise from channel 5 (Figure 18) was used as a signal model with infinite apparent horizontal velocity. In this way, the signal was "shaped" in frequency to agree with the measured noise, and the possibility of having simple single-channel frequency filtering incorporated in the filter set was reduced. Two percent random noise was added to the noise model to decrease the effect of the extremely high noise correlation between individual sensors.

Time-domain operators for these filters are shown in Figure 20.

2. Ensemble Filter

As soon as preliminary results indicated that the above filter could successfully reject the major component of road noise, a second filter set was developed. This set combined the high-noise sample with four samples representing periods of "normal" noise activity. The method of development was essentially the same as that presented above.

Time-domain operators for this set are presented in Figure 21. The amplitude response of this filter is shown in Figure 22. Maximum dynamic range over a relatively narrow band of frequencies has been limited to something less than 40 db. Therefore, these filters should be physically realizable in the analog system.

---

*Ibid. p. V-2

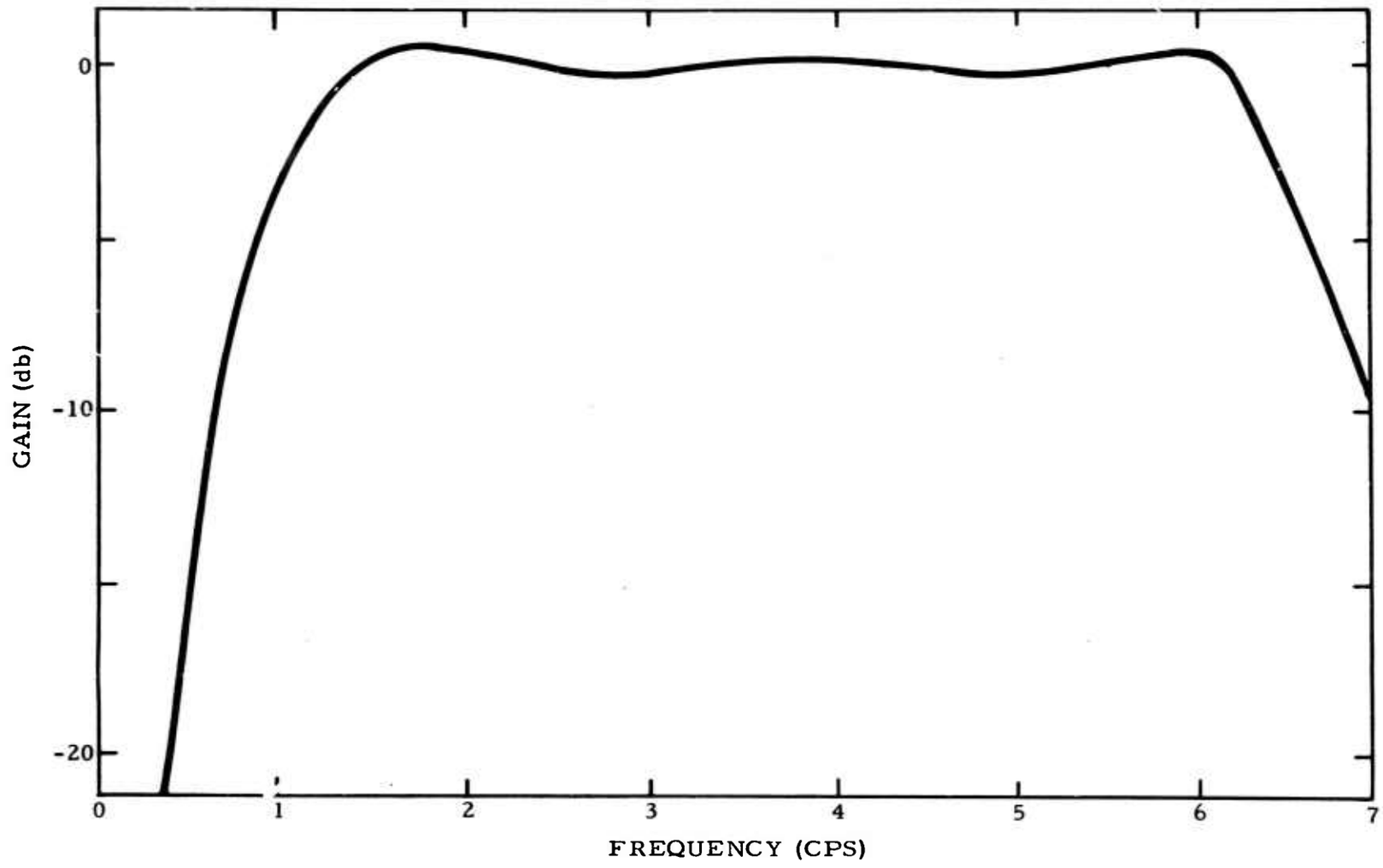

Figure 19. Frequency Response of Prewhitening and Antialiasing Filter

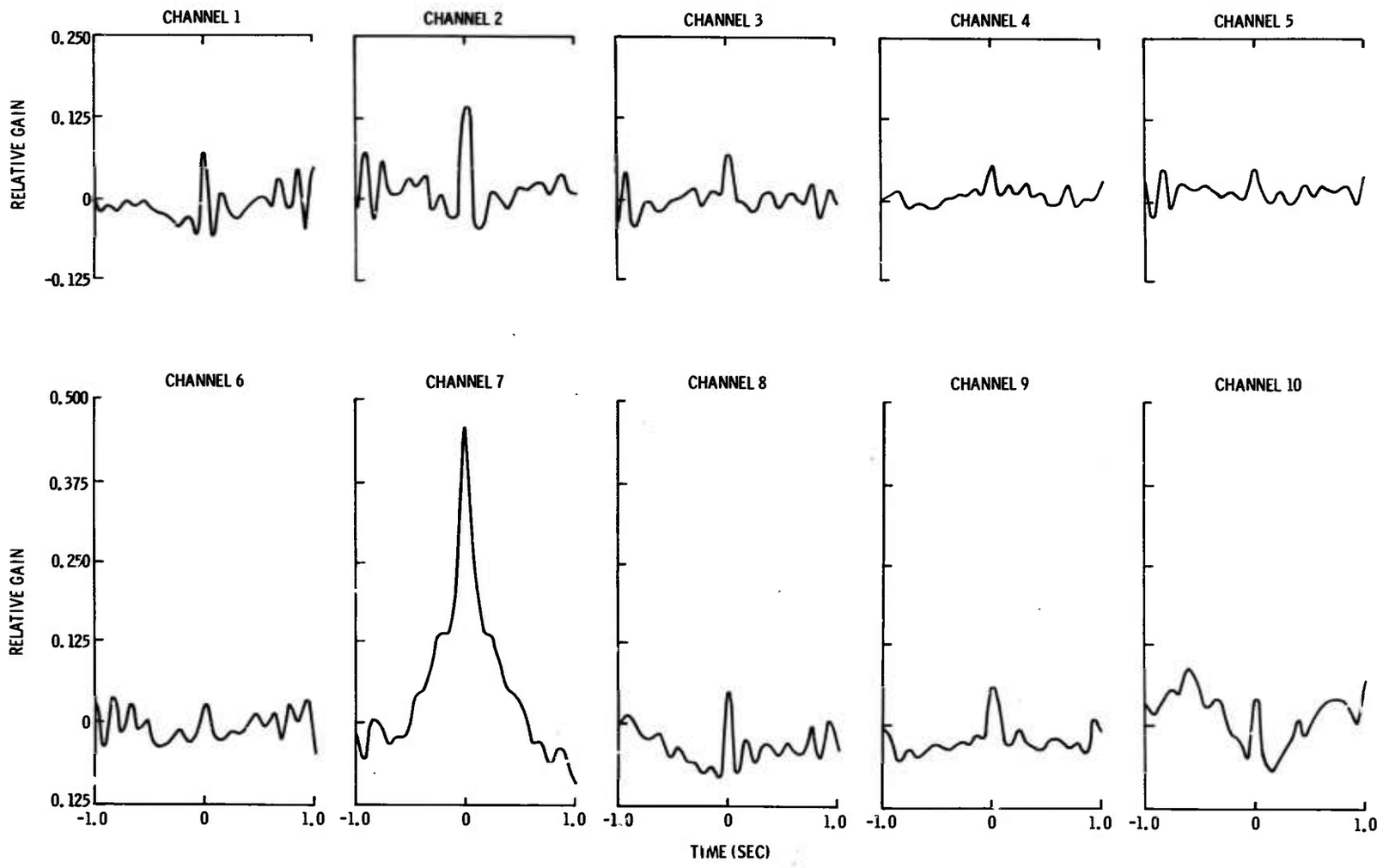

Figure 20. Time-Domain Operators for 10-Channel, 27-Point Filter, Developed from a Single High-Noise Sample

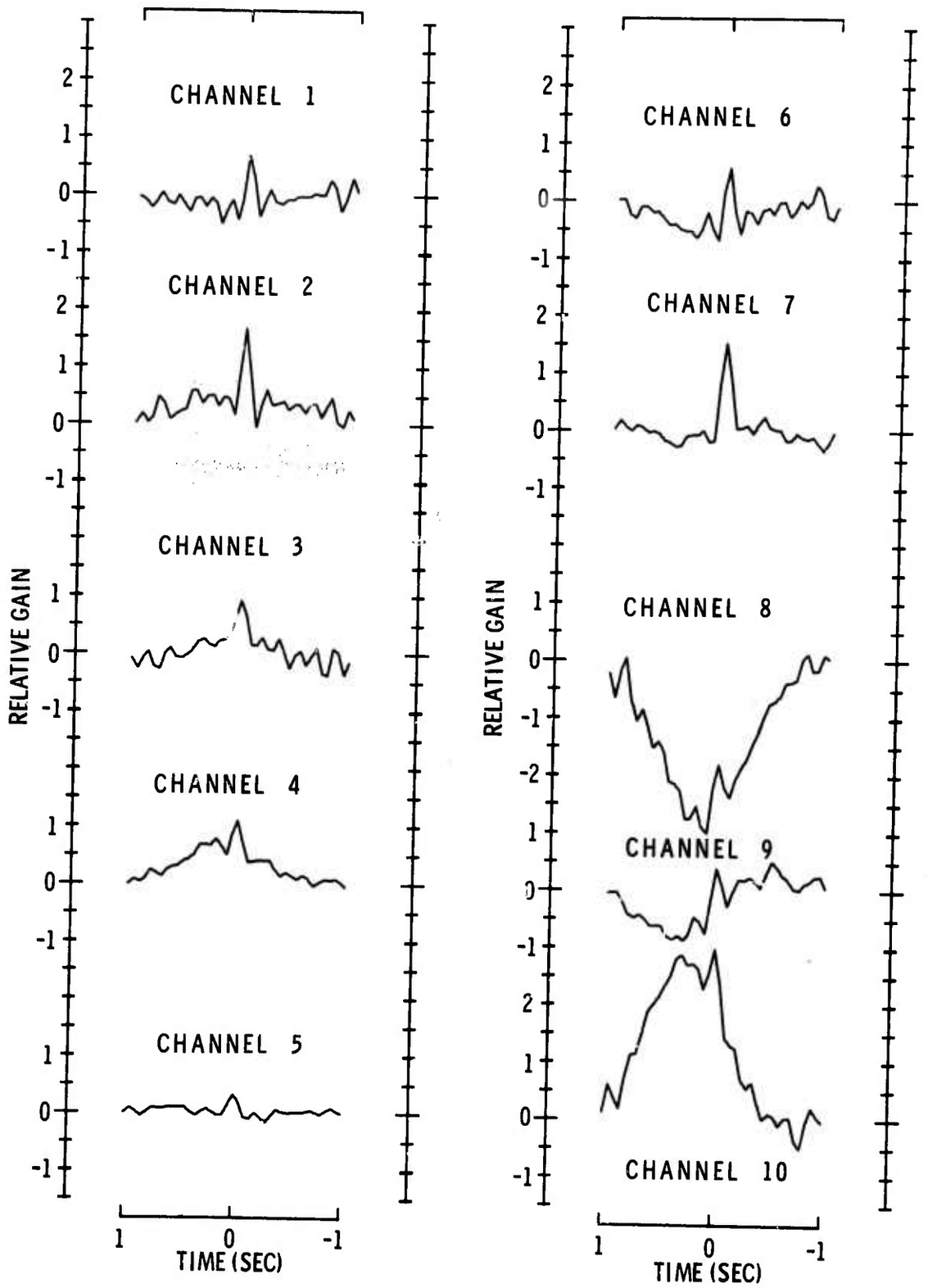

Figure 21. Time-Domain Operators for MCF-11, 27 Point Filter

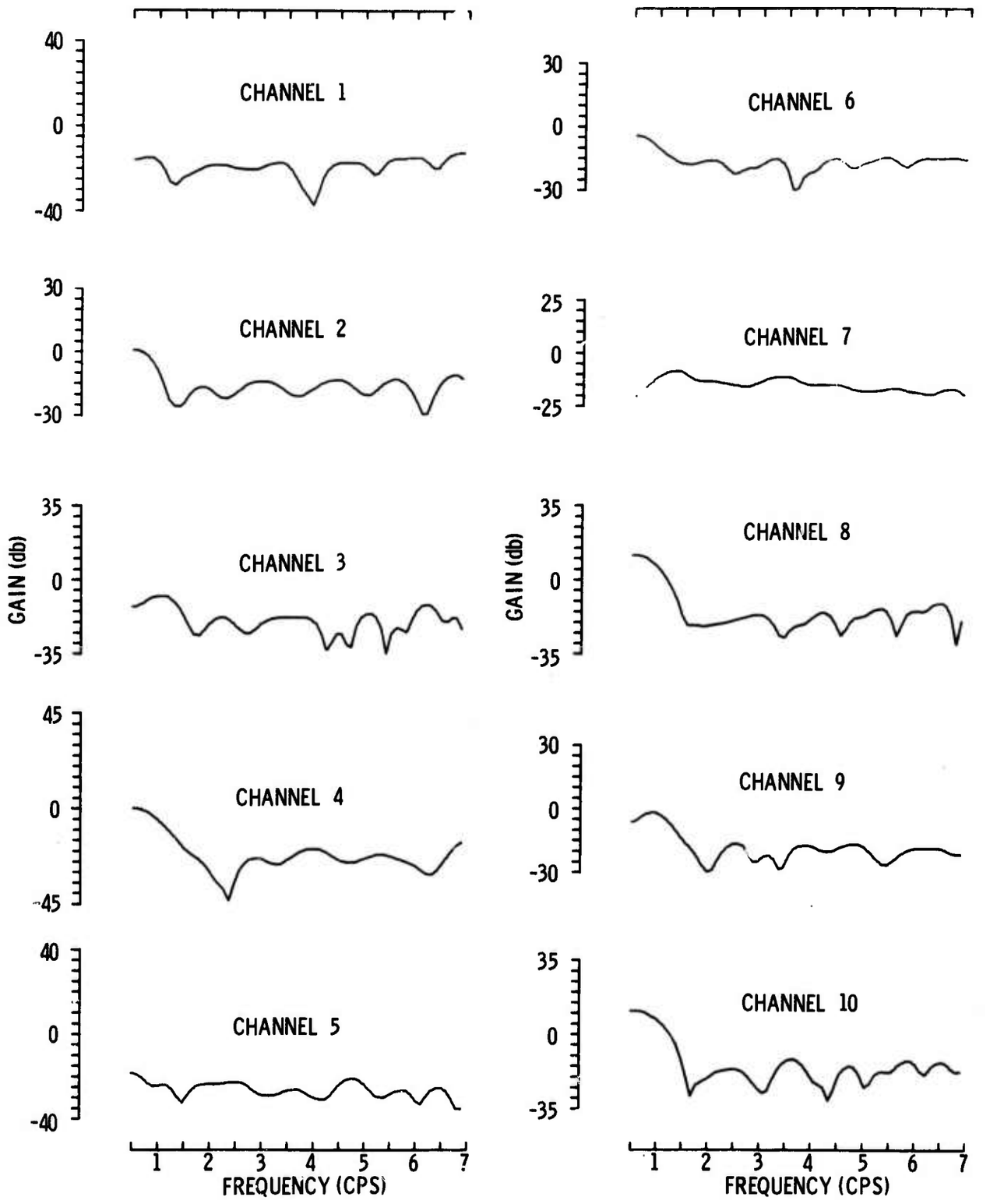

Figure 22. Amplitude Response of MCF-11

SECTION V

THEORETICAL FILTER EVALUATION

Both sets of filters were evaluated on the IBM 7044. Evaluation of set 2, designated as MCF-11, is more complete because this is the filter which has been installed on-line.

A. HIGH-NOISE FILTER

It was intended that this filter should be designed to maximize rejection of the particular noise in question. Because only one noise sample was used in the design and evaluation, the results may be considered optimum. Figure 23 depicts the actual noise sample on traces 1 through 10. Trace 11 is a prediction estimate of trace 10 based on the information contained in traces 1 through 9. Trace 12 is a simple summation of the first 10, and trace 13 is the MCF output.

Signal-to-noise improvements were computed by comparing the ratio of a filtered spike (SF) and filtered noise (NF) to the ratio of a summed spike (SS) and summed noise (NS). The ratios of the filtered traces and the summed trace were also compared with the ratio of a reference spike (SR) and reference noise (NR) taken from channel 5. Using this abbreviated form, the following improvements were derived:

- S/N of filtered data to summed data = $\frac{SF/NF}{SS/NS}$
- S/N of filtered data to reference data = $\frac{SF/NF}{SR/NR}$
- S/N of summed data to reference data = $\frac{SS/NS}{SR/NR}$

These three curves are pictured in Figure 24.

Because only one noise sample was used in the filter design and the filter was subsequently applied to this sample, the overall signal-to-noise improvement was very good. In the particular frequency band of dominant road noise, a signal-to-noise improvement of 27 db was realized when the filtered data was compared with reference data from channel 5. A visual comparison of trace 10 and its predicted estimate (trace 11) indicates that these results might be expected (Figure 23).

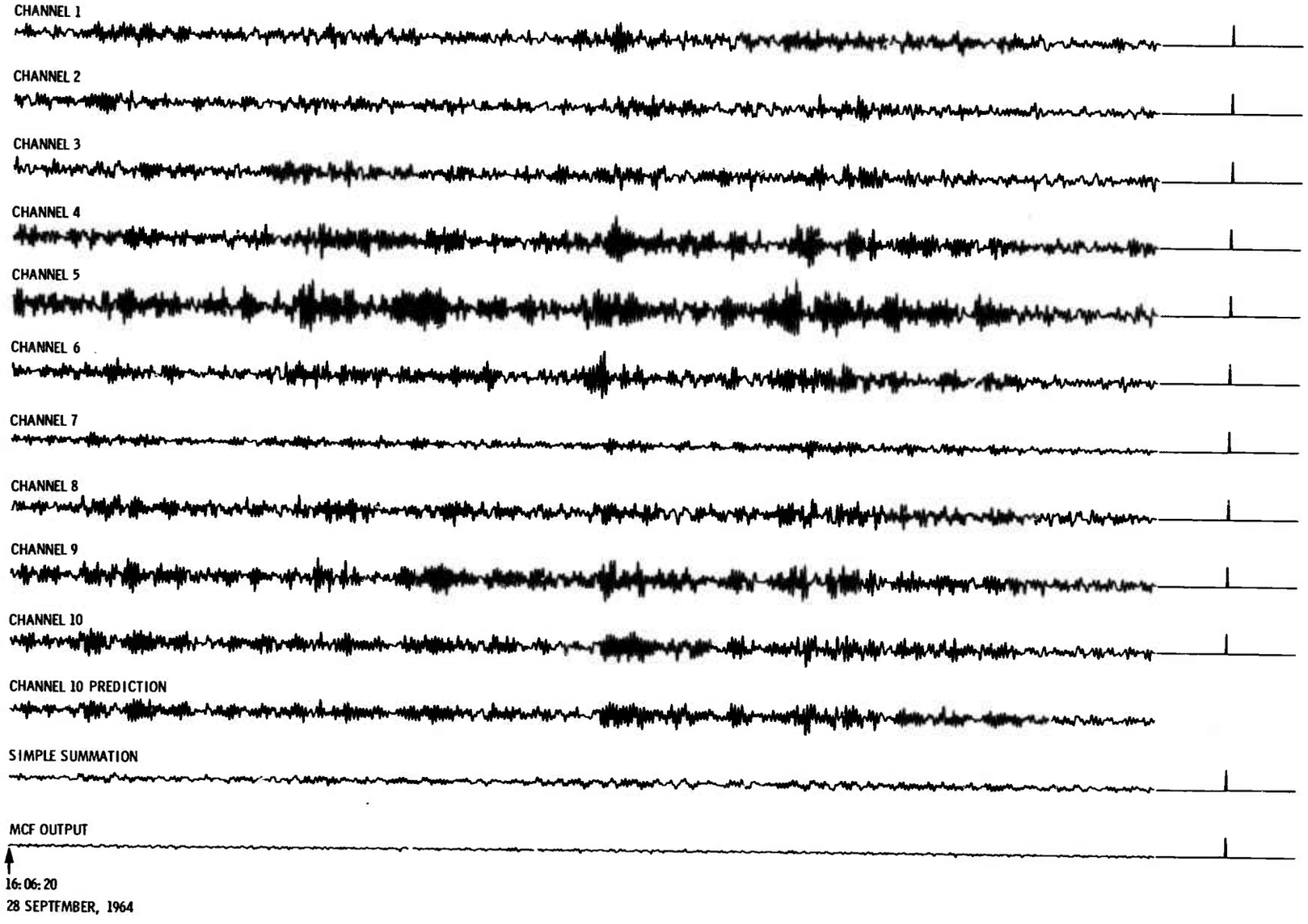

Figure 23. Resampled High-Noise Sample with Prediction Estimate Simple Summation and Filtered Traces (High-Noise Filter)

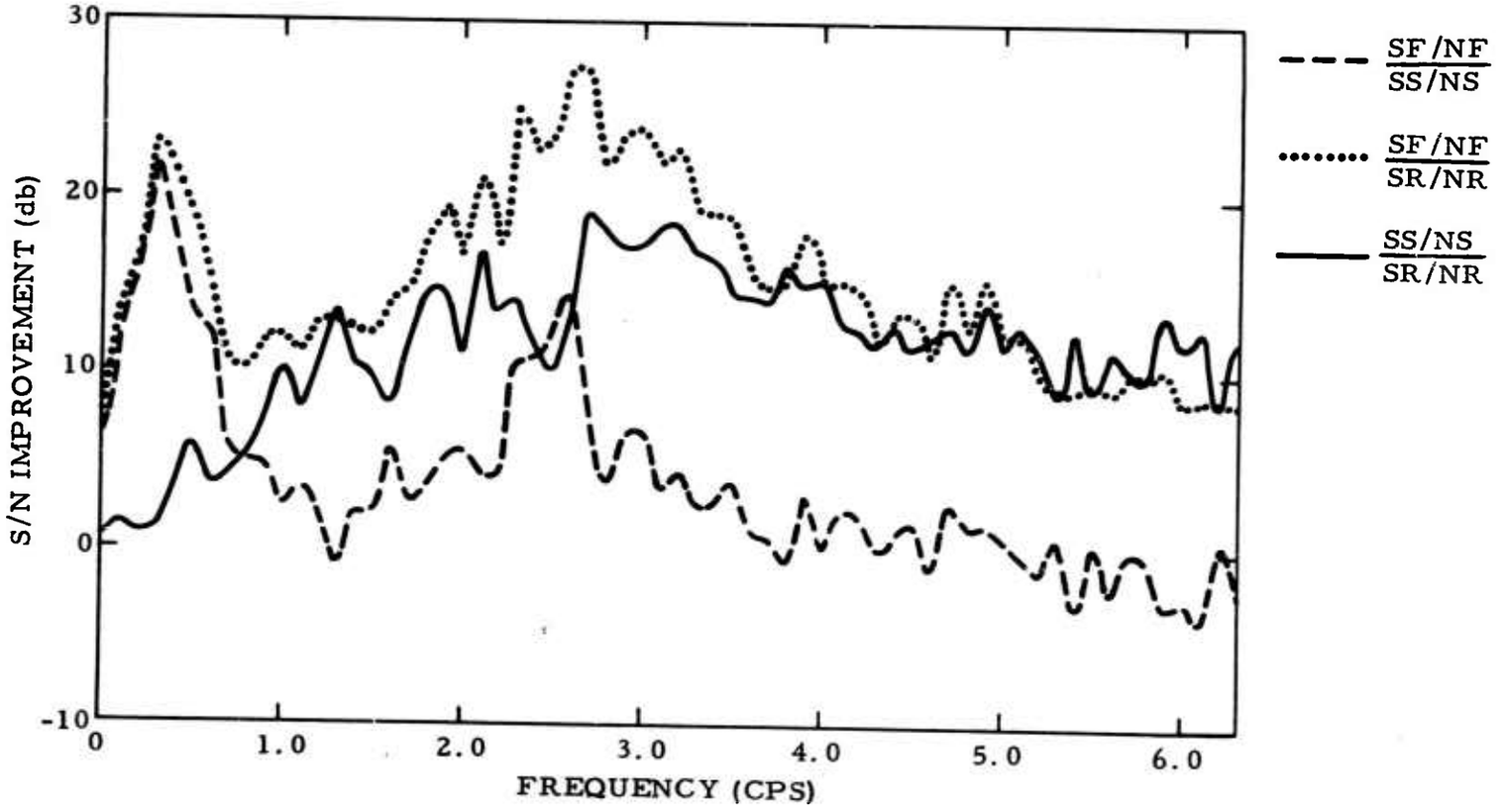

Figure 24. Signal-To-Noise Improvement Curves Comparing Filtered, Summed and Reference Data

As a further check on the effectiveness of the high noise filter, a real signal was added to the high noise sample. The MCF was subsequently applied, and the result is shown in Figure 25. Again it is obvious that the filtered output is superior to the straight summation. The noise rejection ratios presented in Figure 26 substantiate this observation. The designation N is used to represent the noise with signal added.

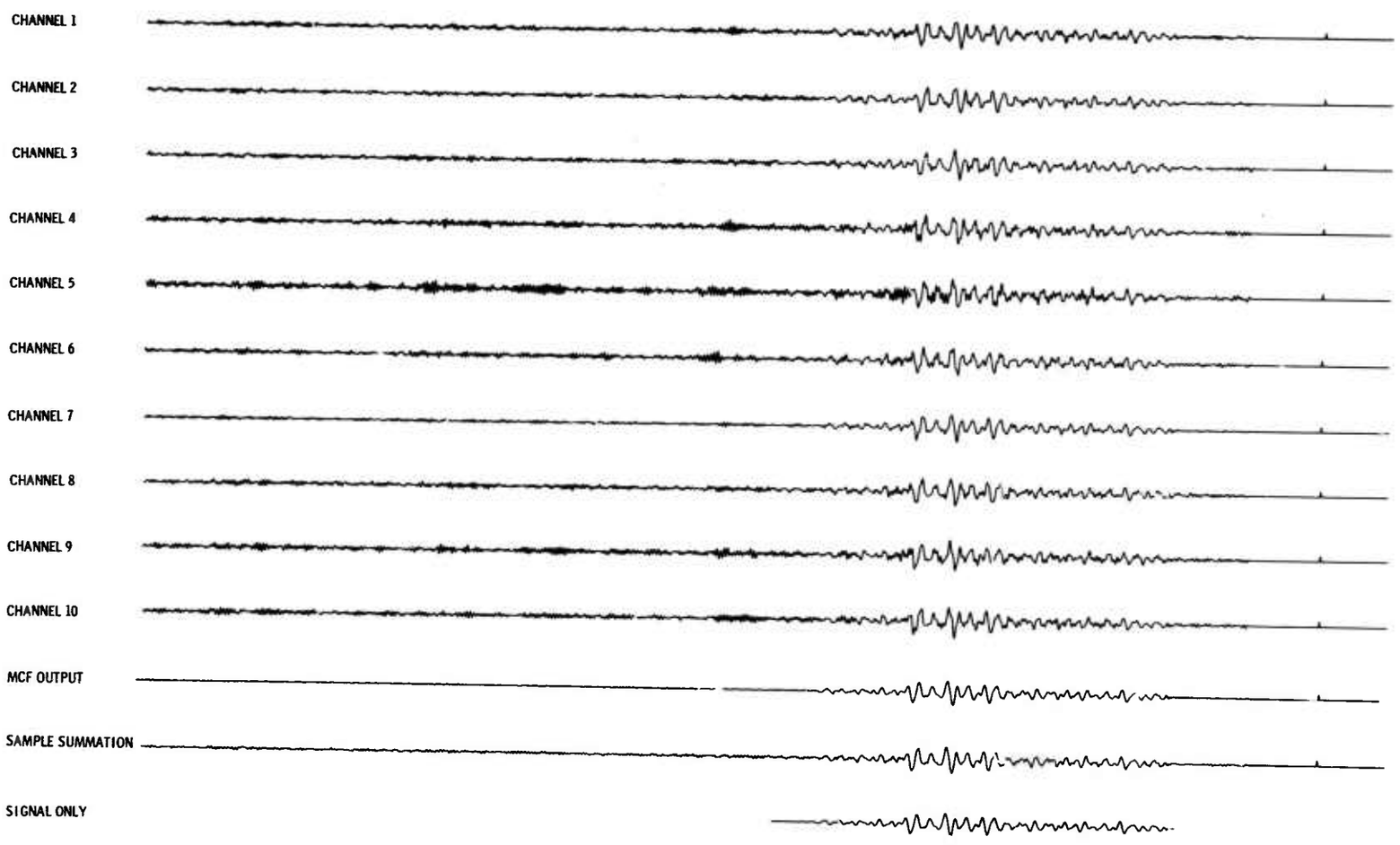

Figure 25. High-Noise Sample With Actual Signal Added

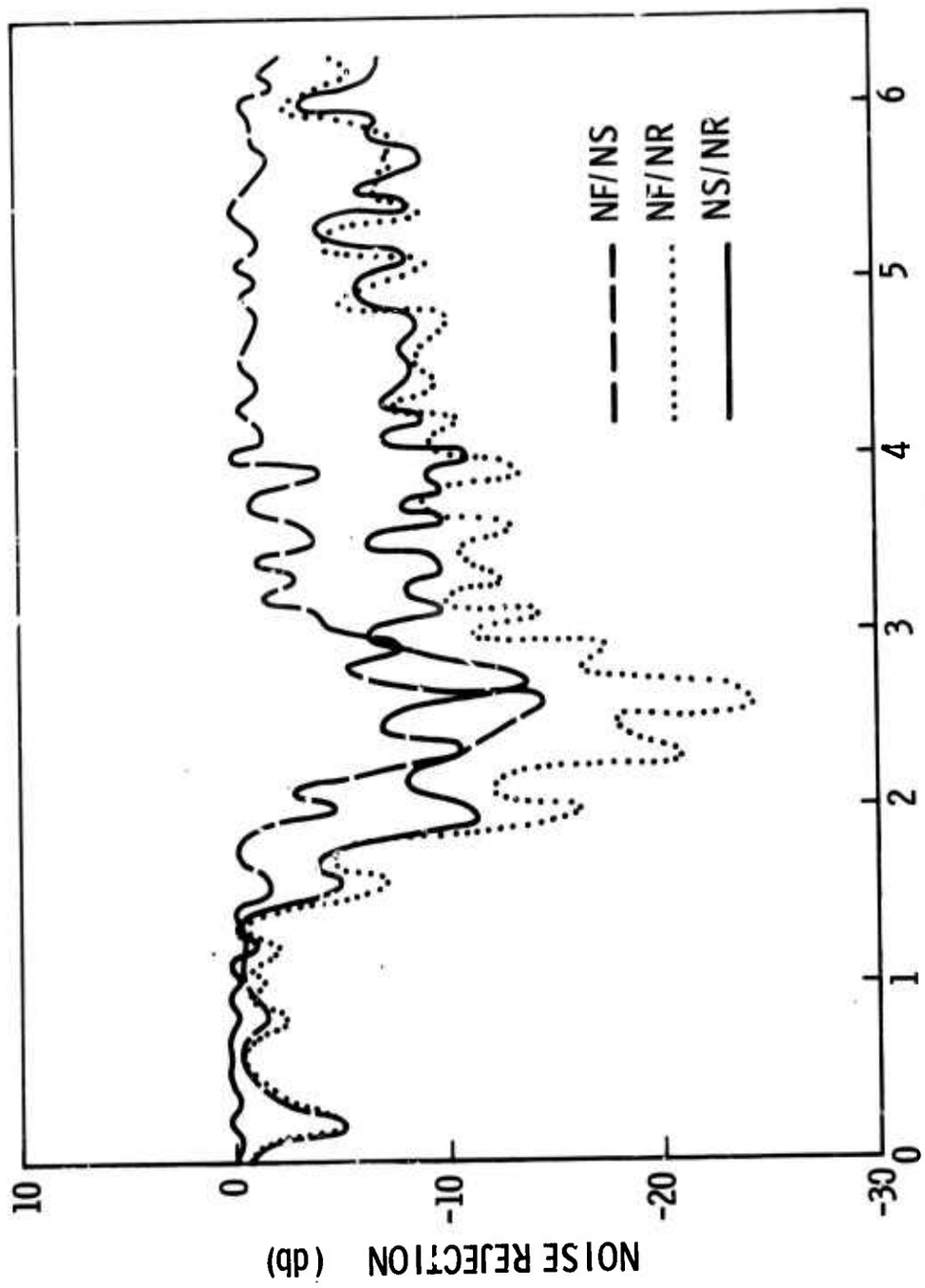

Figure 26. Noise Rejection Using "Road Noise" Filter

B. ENSEMBLE FILTER

The ensemble designed filter was applied to the high-noise sample discussed previously and to a normal noise sample not included in the design ensemble. Figures 27 and 28 depict these samples on traces 1 through 10. Trace 11 is the prediction estimate of trace 10. Trace 12 is the difference between trace 10 and its estimate and is designated as prediction error. Traces 13 and 14 are the simple summation and MCF output, respectively.

As before, the filter is able to reject a significant portion of the road noise. The prediction error trace on the high-noise sample is quite low in amplitude, indicating that the noise is coherent and can be predicted fairly well. The MCF output has noticeably lower amplitude than the simple summation and thereby is more desirable.

Signal-to-noise improvement curves for the two noise samples are presented in Figures 29 and 30. Prediction error-to-channel 10 noise power ratios are shown in Figure 31.

The signal-to-noise improvement realized when the filtered normal noise was compared with the reference noise is no better than a simple summation-to-reference noise signal-to-noise improvement above 1.0 cps. In fact, at higher frequencies the simple summation appears to do a better job of noise rejection. This is not unusual considering the severity of the rejection necessary in the relatively narrow band of road noise energy. To enable the filter to meet this requirement, a trade-off was necessary at other frequencies and a pseudosimple summation resulted.

Figure 32 shows the random noise response of the filter and substantiates the theory that the filter approximates a simple summation above 1.2 cps. The response of a simple summation of 10 channels of completely random noise should be -10 db (or $\frac{1}{\sqrt{10}}$).

C. EVALUATION SUMMARY

Based upon the preceding data, it appeared that MCF-11, when installed on-line, would have limited utility as follows:

- Ambient road noise should be rejected by about 20-25 db in the frequency band of dominant energy
- During times of normal noise activity, when no road noise is present, the filter should perform somewhat better than a simple summation below about 1.0 cps
- Above 1.0 cps the filter should approximate a simple summation

Overall, it appeared that MCF-11 would perform better than the filter presently in operation although a trade-off in effectiveness would be necessary to obtain the desired road noise rejection.

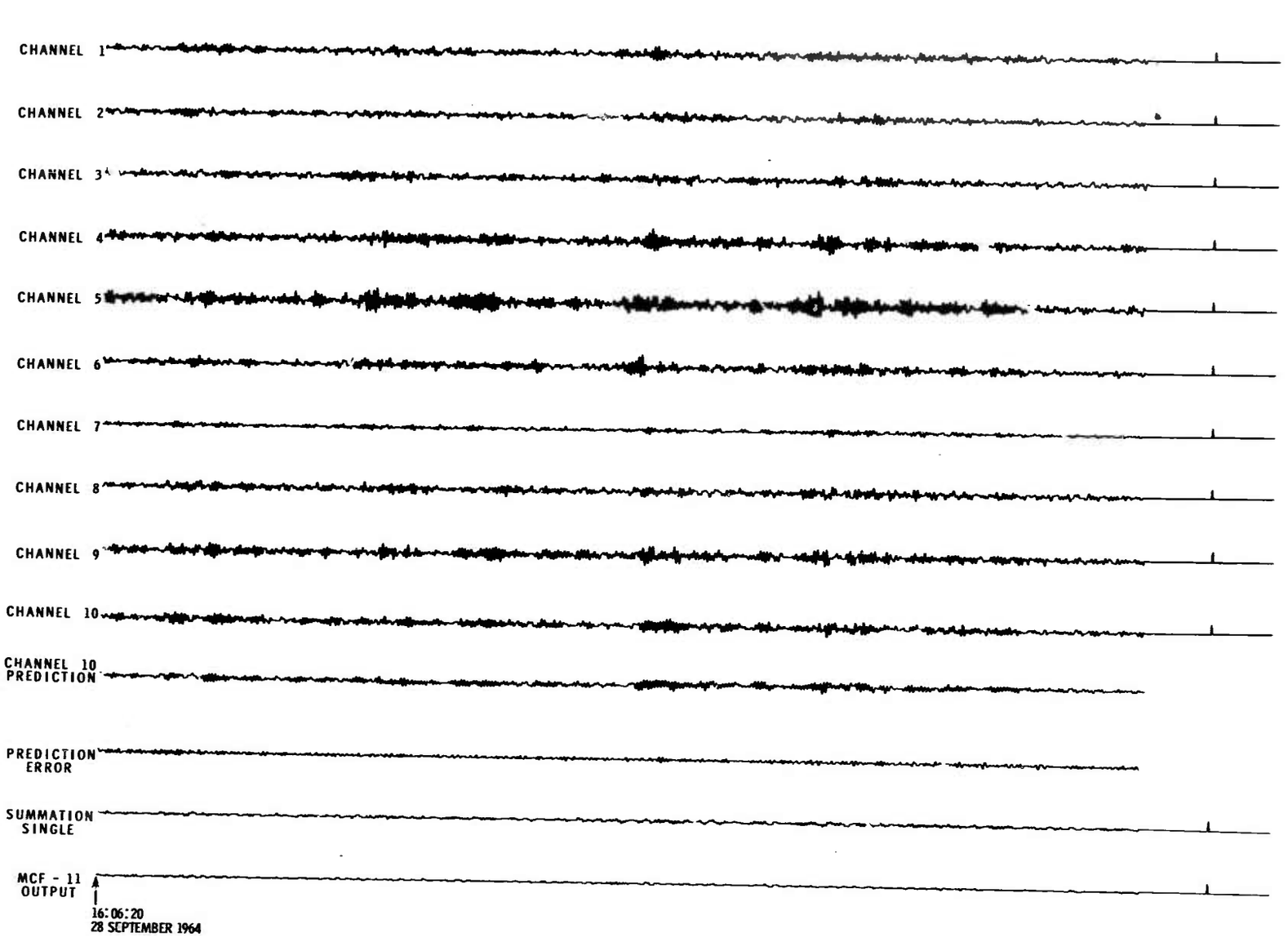

Figure 27. Resampled High-Noise Sample with Prediction Estimate, Prediction Error, Simple Summation, and Filtered Traces (MCF-11)

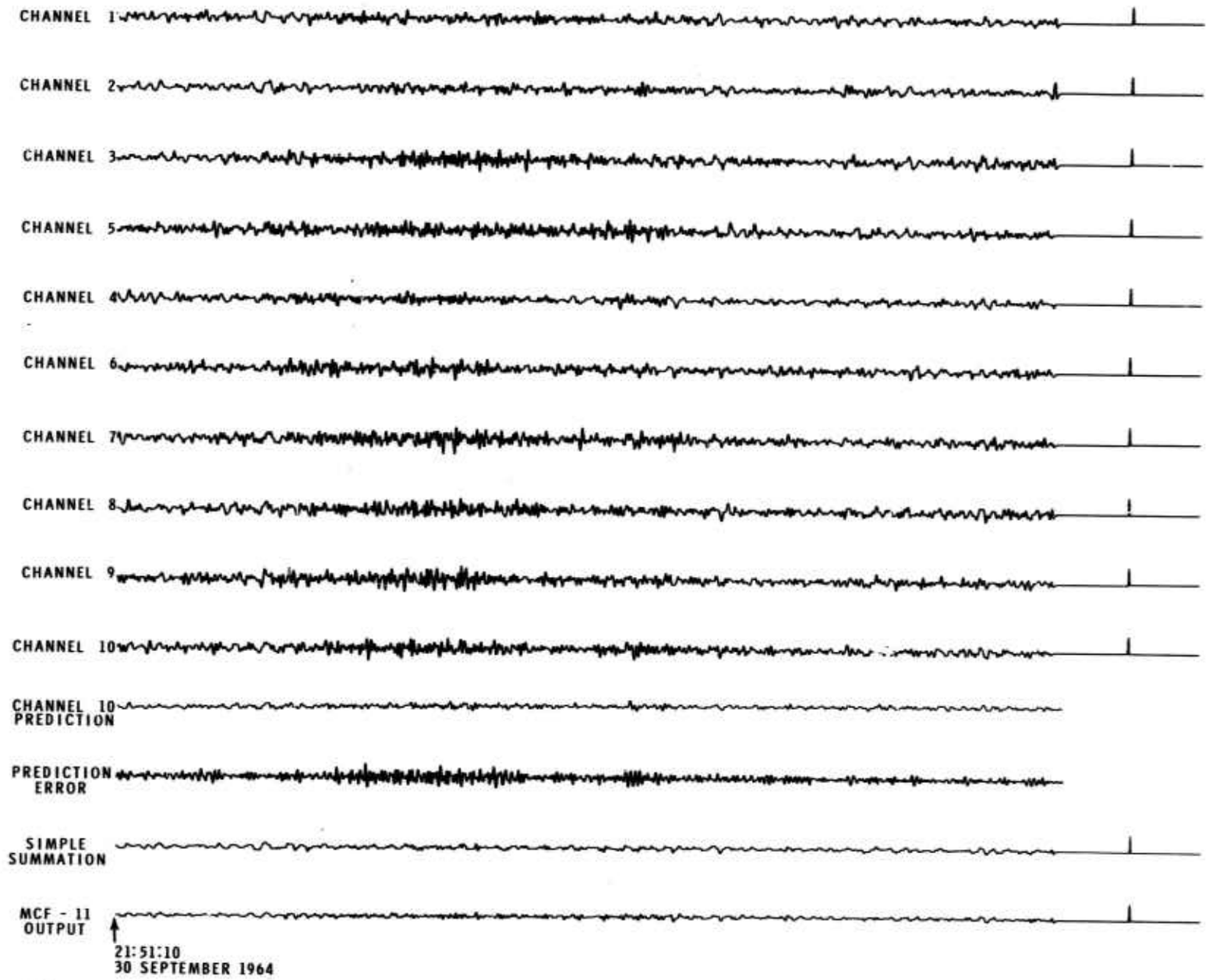

Figure 28. Resampled Normal-Noise Sample with Prediction Estimate, Prediction Error, Simple Summation, and Filtered Traces (MCF-11)

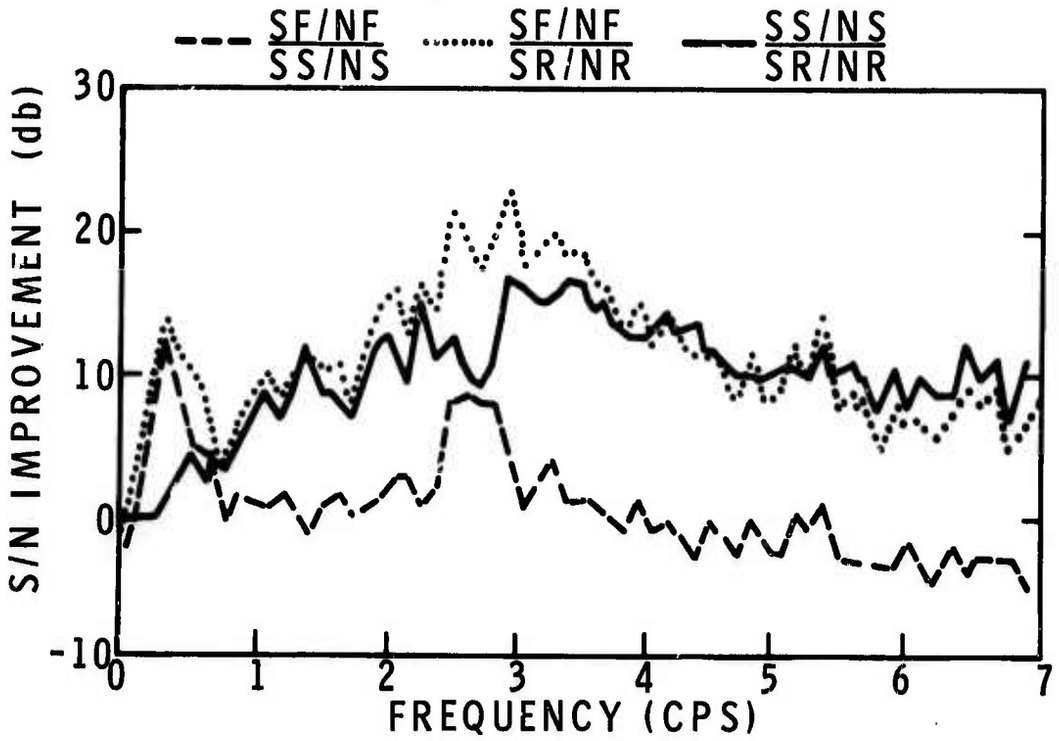

Figure 29. Signal-To-Noise Improvement Curves for High-Noise Samples Comparing Filtered, Summed and Reference Data

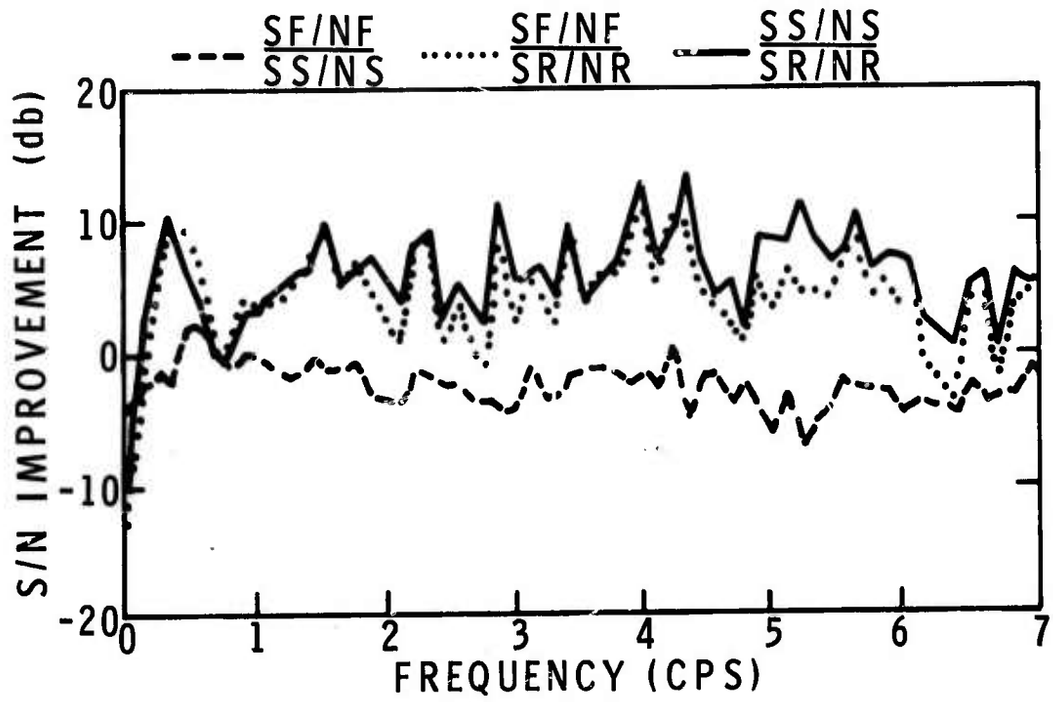

Figure 30. Signal-To-Noise Improvement Curves for Normal-Noise Sample Comparing Filtered, Summed and Reference Data

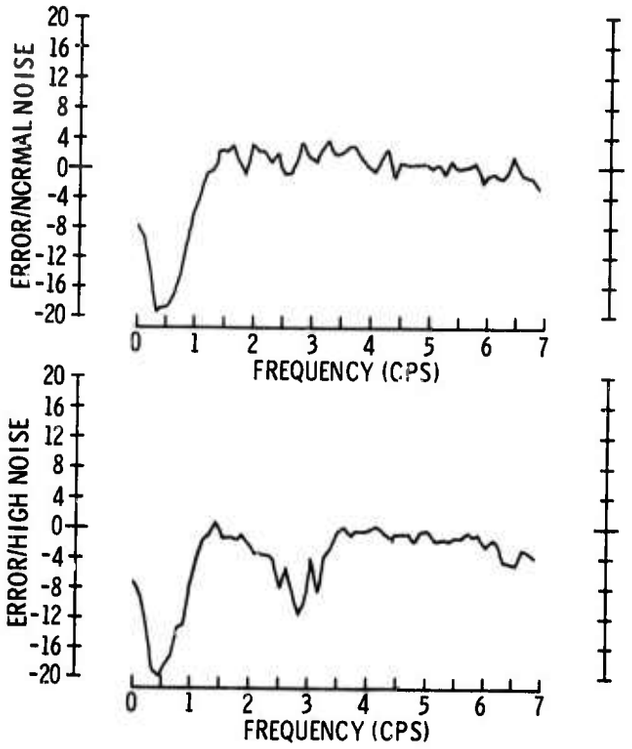

Figure 31. Prediction Error-To-Reference Noise Power Ratios for High-Noise and Normal-Noise Samples

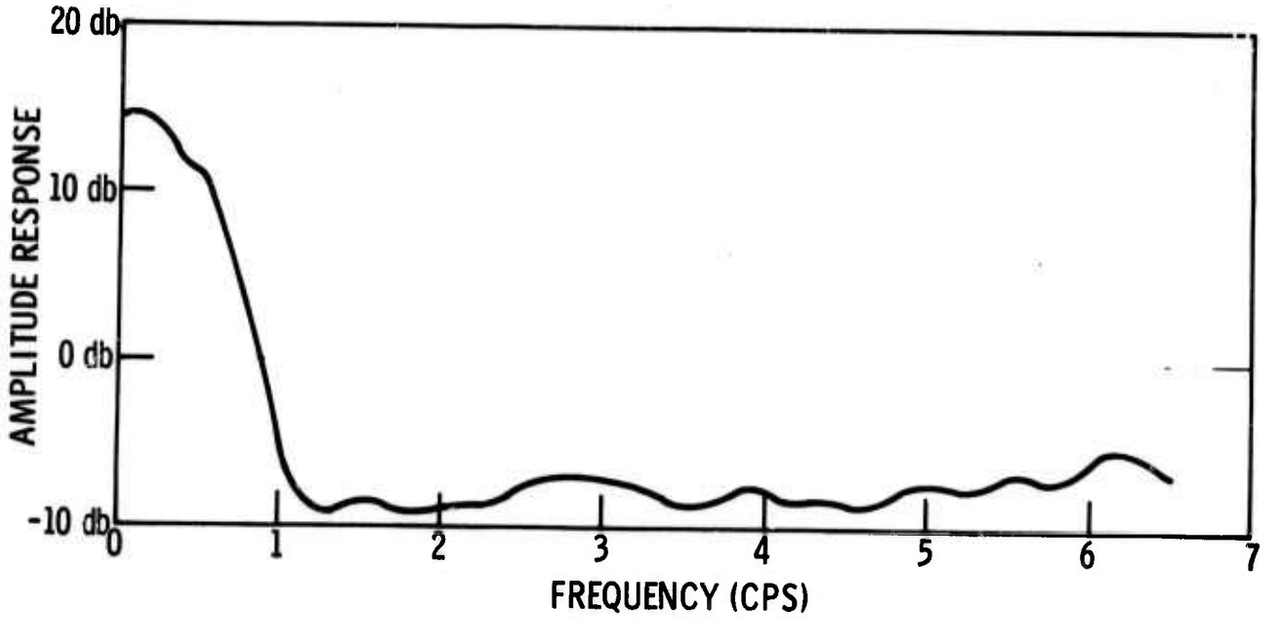

Figure 32. Random Noise Response for 27-Point MCF with "Road Noise" in Design Ensemble

SECTION VI

EVALUATION OF THE ON-LINE PROCESSORS

A limited evaluation of the effectiveness of the analog processors was accomplished using data recorded in late 1965. Five signals and five noise samples were analyzed visually for any obvious irregularities. Timing marks were found on the filtered data and were traced to a feedback from the Develocorders. Otherwise, the on-line filtered data appeared to be quite reasonable with a noise rejection of approximately 5 to 8 db.

A. EVALUATION OF IP-1, IP-2, MCF-9, AND DG 1-4

Because only subsurface data were recorded concurrently with the processor outputs, the evaluation of the surface processor was limited to this visual check. The subsurface processor was evaluated in more detail. One signal and one noise sample were chosen for this evaluation. These were gain-equalized and are presented in Figures 33 and 34. Outputs from the analog processors IP-1, IP-2, MCF-9, and DG 1-4 were compared with equivalent traces which had been filtered on the IBM 7044 using the theoretical filters designed previously. These comparisons are presented in Figures 35 and 36. The similarity of the IBM 7044 and analog processed data indicates that the analog processors are operating approximately as designed.

B. EVALUATION OF THE ROAD NOISE FILTER

The filter designed primarily to reject the road noise at UBO was fabricated and installed on-line by personnel from the Geotechnical division of Teledyne Incorporated. No response curves have been computed since this filter became operational, but preliminary investigations indicate that no significant improvement has been realized over MCF-1 previously installed. The reasons for this are probably twofold. First, the filter (designated MCF-11 in this report) was designed from data recorded at UBO in 1964 and may not be truly representative of present signal and noise statistics. Second, the data ensemble used in the filter design was limited to only five noise samples taken over a very short time span. A better estimate should be possible if personnel at UBO could supply several (approximately 10 to 20) noise samples containing road noise and at least an equal number of samples containing "normal" noise data. These data should be taken over an extended time period of at least one to three months. A multichannel processor developed from data of this type should be far more efficient in rejecting the various noise modes present at UBO.

Figure 33. Signal Sample Used in Evaluation of the On-Line Processors

Figure 34. Noise Sample Used in Evaluation of the On-Line Processors

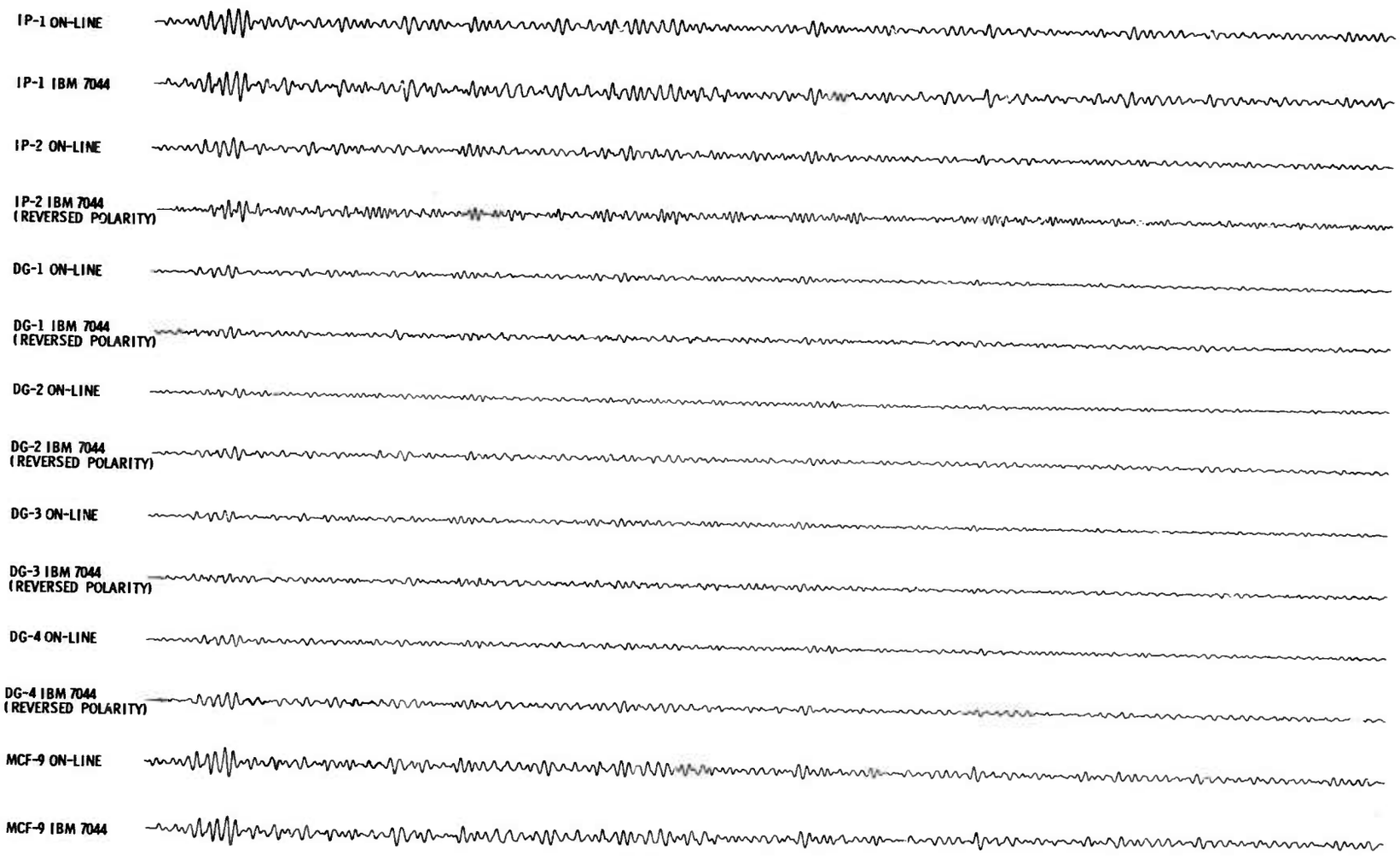

Figure 35. Signal Data Filtered On-Line Compared with the Same Data Filtered on the IBM 7044

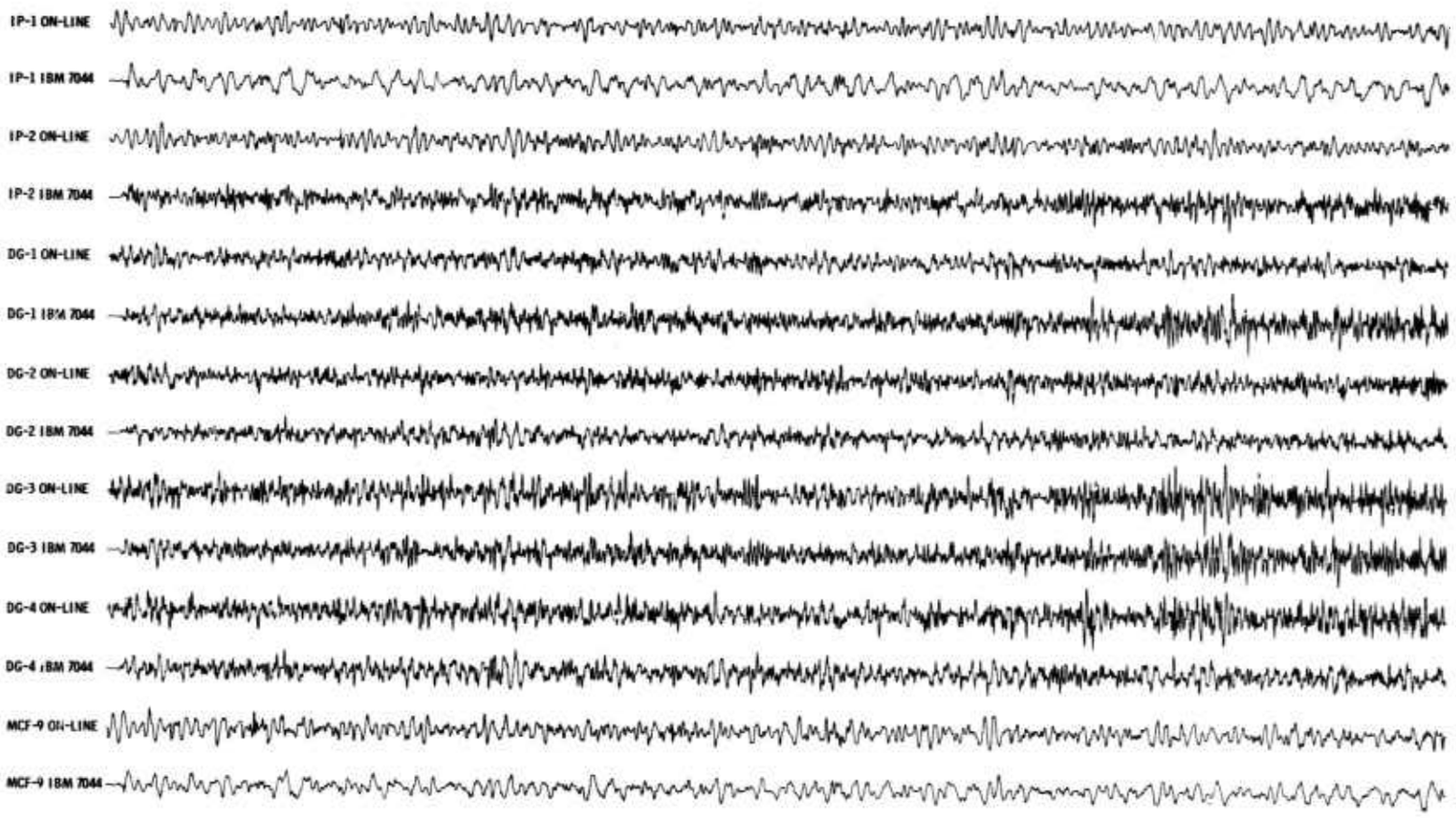

Figure 36. Noise Data Filtered On-Line Compared with the Same Data Filtered on the IBM 7044